Application of the unmanned Offshore Sensing SailBuoy for validation of ocean model simulations and remote sensing data in the North Atlantic

Master thesis in physical oceanography

by
Ragnhild Stegali Borge

December 1, 2015

UNIVERSITY OF BERGEN
GEOPHYSICAL INSTITUTE

Photo on the front page are the unmanned remotely-controlled Offshore Sensing SailBuoy developed by Christian Michelsen Research (CMR) and now produced by Offshore Sensing. (www.sailbuoy.no)

Abstract

The Offshore Sensing SailBuoy, is a remotely controlled, wind driven unmanned ocean vehicle. It sampled near surface properties during a mission in the North Atlantic in June - August 2014. Three parameters were recorded, sea surface temperature, conductivity and dissolved oxygen concentration.

The observed near surface properties are compared with ocean model output and remote sensing data. The mean error of sea surface temperature data from remote sensing and ocean models compared with near surface measurements from the SailBuoy are approximately $0.5°C$.

For sea surface salinity, the mean error from ocean model outputs compared with sea surface salinity calculated from the conductivity measured by the SailBuoy, are approximately 0.3 psu.

The SailBuoy can measure salinity near the coast, where remote sensing data are not available.

It has the capacity to be a cost- and time saving alternative to larger research vessels, as well as for validation of ocean model simulations and remote sensing data.

Acknowledgements

I want to thank Lars R. Hole for being an inspiring supervisor guiding me through this master project. Thanks for all the help, encouragement, proof reading and guiding through programming issues. There has always been time for my questions. I would also like to thank my co-supervisor Knut Barthel for your good advice.

Access to data has been crucial to implement this thesis. Thank you to David Peddie for the access to data from the Offshore Sensing SailBuoy, and thank you to the MyOcean project for available ocean model output and remote sensing data.

This thesis had not been possible without the support from my family. Thank you to my lovely husband, Thor, and my two children, Maja and Tobias. You are my sunshine whenever I feel lost or distraught.

Thank you to my Mom and Dad who has taken their share of childcare and always supported me. Dad, you are my superhero, and Mom, thanks for the best hugs and the right words when I needed it the most.

Finally, thanks to all my co-students at the Geophysical Institute, for all the good times. It has been an adventure.

Contents

List of Figures

List of Tables

Chapter 1

Introduction

The ocean surface is a complex air-sea interface. It sets the boundary conditions for physical processes and plays a key role in the global atmosphere-ocean energy balance (Paskyaci and Fer 2010). Having a better understanding of the processes of momentum, heat and gas exchange between the atmosphere and the ocean, is important to get a better description of the ocean's role in climate. Sea surface temperature (SST) and sea surface salinity (SSS) are essential parameters for understanding the atmosphere-ocean balance, as well as large-scale ocean and atmospheric circulation. Salinity toghether with temperature determines buoyancy. The buoyancy is important for understanding the thermohaline circulation, the density driven ocean circulation (Le Vine et al. 2010). Near surface dissolved oxygen has a diurnal variation. It responds to physical changes, as temperature and salinity, and biological changes caused by production of oxygen during photosynthesis and a loss during respiration and decompositions. The possibility to measure near surface oxygen can give an indicator of environmental changes in the ocean. For understanding the physical mechanisms and processes, calibration of satellite data and numerical models and measurements of near-surface properties of the ocean are crucial (Ghani et al. 2014).

Independent observation methods of hydrographic properties of large ocean areas have been outfitted since the 1990s. Key systems such as buoys with CT (conductivity and temperature) sensors, have been used for temperature and salinity measurements, using different radio and satellite communication systems. For the possibility of two-way communication, such platforms now uses the Iridium System and a wider bandwidth to increase the possibility to carry multiple sensors such as near surface dissolved oxygen (Ghani et al. 2014). For oxygen measurements, Körtzinger et al. (2005) reported the first study results, high quality measurements from two floaters equipped with optode sensors for oxygen measurements.

During the last decade, several autonomous observing systems have been developed, as well as platforms and sensors. The oceanographic platforms are characterized as autonomous or as unmanned vessels due to how they operate. They may track large ocean areas measuring oceanographic, as well as meteorological properties and transmit data through satellite or radio. It may navigate to a specific way point or location, and change sampling rate during the track period (Perry 2003).

A brief discussion in the development of autonomous vessels in Caccia et al. (2008) list several unmanned vessels. The first autonomous surface vessel "ARTEMIS" was developed through MIT Sea Grant Collage program in 1993 (Manley 1997)and demonstrated way point navigation of autonomous sampling of hydrographic data. Examples of autonomous vessels developed in Europe are "the measuring Dolphin" developed by the university of Rockstock (Germany) (Majohr and Buch 2006). "Delfim", a autonomous catamaran developed by the DSOR lab of Lisbon IST-ISR (Pascoal et al. 2000).Catamaran "Charlie", by CNR-ISSIA Genova (Italy) developed for sampling sea surface micro-layer (Caccia et al. 2005), "ROAZ" developed by Autonomous Systems Labratory at ISEP-Institute of Engineering of Porto (Martins et al. 2006) and the autonomous catamaran "Springer", for tracking pollutants developed by (Xu et al. 2006).

A challenge with unmanned vehicles is the power it needs for a propel, and the operating time may be limited. In order to collect data with an unmanned vehicle over a longer period of time, energy can be retrieved from the waves, sun or wind (Peddie 2011). Examples are the wave powered Wave Glider designed by Liquid Robotics Sunnyvale California (http://www.liquidr.com/technology/waveglider/how-it-works.html), the wind powered SailDrone (http://mstfoundation.org/story/Saildrone), using a wind-propel and C-Endron (http://asvglobal.com/product/c-enduro/) using solar energy (Ghani et al. 2014).

The main aim of this thesis was to investigate and increase the understanding of usefulness of an unmanned surface vehicle and validate ocean model output and remote sensing data. In this thesis the Offshore Sensing SailBuoy (www.sailbuoy.no) developed by Christian Michelsen Research (CMR) and now produced by Offshore Sensing is used. The SailBuoy navigates toward given way points without a propel, but as a 100 % wind driven platform. By comparing data from the SailBuoy with numerical ocean model output and remote sensing data, the usefulness can be investigated and its possibility to verify data from remote sensing and numerical ocean models. Data from a field campaign, from 26 June 2014 to 14 August 2014, in the North Atlantic is used. This is an area that can have strong currents and high wind, and it is important to evaluate the preformance of the SailBuoy in such conditions. This campaign is also influenced by ocean futures as the Norwegian Coastal Current. Current maps all the way back to the nineteenth century show the northward flow outside Norway (Sætre 2012). When the SailBuoy leaves coastal areas, the water masses will be influenced by Atlantic water with

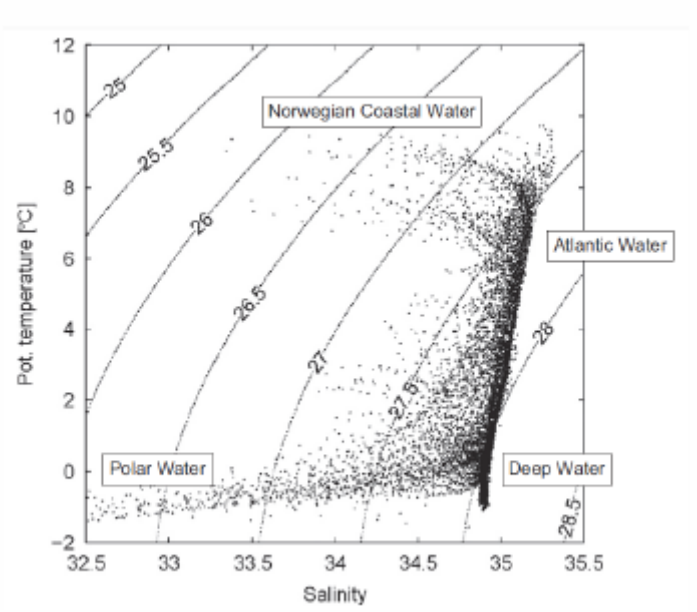

Figure 1.1: Temperature - Salinity diagram presenting the main water masses in the Nordic Sea (Høydalsvik et al. 2013).

contrasted characteristics, and fronts may be found. The inflow of Atlantic water from the North Atlantic Current is important for the climate in Northern Europe (Sundby 2004). Figure 1.1 present a Temperature-Salinity diagram of the main water masses in the Nordic Sea (Høydalsvik et al. 2013).

Changes in ocean temperature are caused by fluxes of heat across the air-sea boundary and changes in salinity can be explained by changes in the freshwater supply, evaporation, precipitation as well as freezing and melting of ice (Brown et al. 1995). The weather conditions in summer 2014 was unusual with domination high pressure over Scandinavia. From June to August the mean temperature was $2.3°C$ above normal (www.met.no/klima). Figure 1.2 presents the air pressure for 25 June, 2 July, 11 July and 23 July 2014, illustrates a dominating high pressure over Scandinavia with in the campaign period.

The thesis is organized as follows: Chapter 2 is a description of the area of interest, the Norwegian coast and the Greenland-Scotland Ridge. Chapter 3 contains a description of the Offshore Sensing SailBuoy, the field campaign, the equipped sensors on the SailBuoy and the data process. The models used for validation are described in Chapter 4. Chapter 5 contains a description of the sources of remote sensing data used for comparison. The results from the mission are presented in Chapter 6 and discussed in Chapter 7. Finally, a short summary and outlook are provided in Chapter 8.

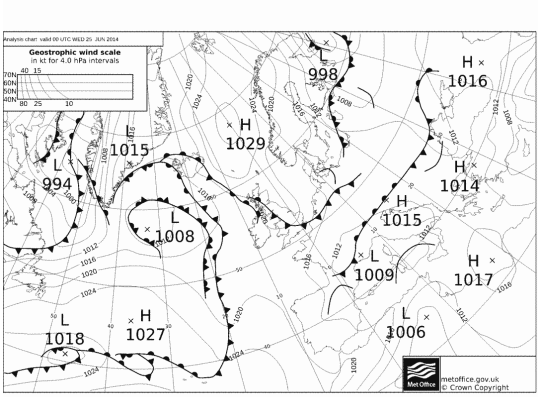

(a) 25. June 00 UTC.

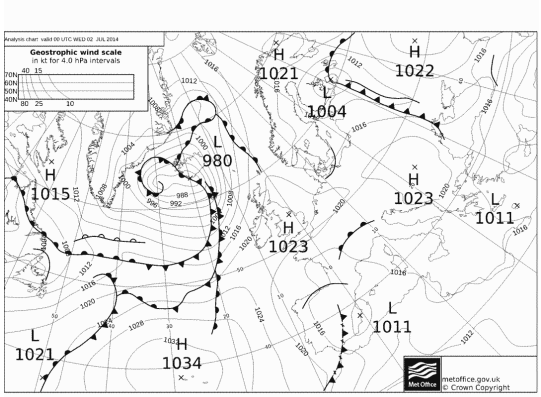

(b) 2. July 00 UTC.

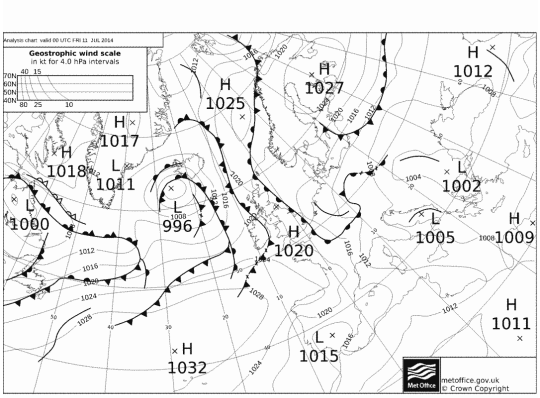

(c) 11. July 00 UTC.

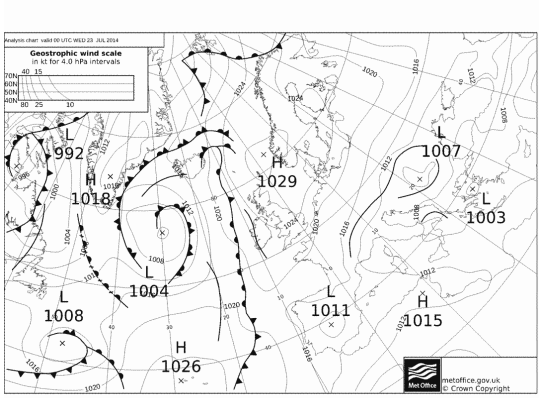

(d) 23. July 00 UTC.

Figure 1.2: Air pressure charts from UK Metoffice, valid at 00 UTC on 25. June, 2. July, 11. July and 23. July 2014. Downloaded from http://www.wetterzentrale.de/topkarten/tkfaxbraar.htm.

Chapter 2

Area

This thesis describes and discusses a field campaign in the North Atlantic, 26 June 2014 to 14 August 2014, from the coastal western Norway towards Iceland. The track is presented in Figure 3.2. This region contains water masses with different characteristics, coastal water along the Norwegian coast and Atlantic water from the North Atlantic Current through the Greenland-Scotland Ridge, see Figure 1.1. In this chapter a description of the Norwegian coast water properties and the Atlantic water inflow is presented.

2.1 Norwegian coast

The first known description of physical conditions on the Norwegian coast and Sea is found in Kongespeilet (The Royal mirror) which was written in 1250 probably by an archbishop in Trondheim. The textbook contains information about seasonal variations in oceanographic parameters as wind, tides and current, but also sailing advice and information about spawning behavior of fish (Sætre 2007).

Temperature and salinity observations in the surface layer along the Norwegian coast started in 1936. For the Norwegian coast, Sætre (2007) concludes that the maximal temperature between 25 July and 5 September, and a minimum between 15 February and 5 April. Salinity maximum occurs during the winter, between December and April and minimum between May and October. The minimum during the summer months are related to freshwater outflow to the coastal current.

2.1.1 Norwegian North-Atlantic Expedition

The 1870's was the time for the first major Marine scientific explorations. The British Challenger (1872-1876) is considered as the first. For Norwegian marine research, the Norwegian North-Atlantic Expedition (1876–1878) is deemed as the most important (Sætre 2012). Justifications and motives for this rather expensive expedition were a combination of scientific and national political motives, navigation and weather forecast and practical-economic motives related to fisheries. The initiators of this expedition was the physicist and meteorologist Henrik Mohn and biologist Georg Ossian Sars (Sætre 2007).

Henrik Mohn was an important person in oceanography and is considered as the founder of physical oceanography and meteorology in Norway. He was the first to develop a mathematical tool to calculate the currents based on the internal mass distribution. In 1866, the Meteorological Department was established and Mohn was the leader of this institute for nearly 50 years (Sætre 2012). Mohn stock a current map of the Norwegian Sea calculated by the mean wind situation and internal distribution of water masses under the Norwegian North-Atlantic Expedition. This mainly showed north and northeast consistently flow in the Norwegian Sea off the Norwegian coast, see Figure 2.1 (Sætre 2007). This illustrates that there was a general understanding of the currents along the Norwegian coast as early as the nineteenth century.

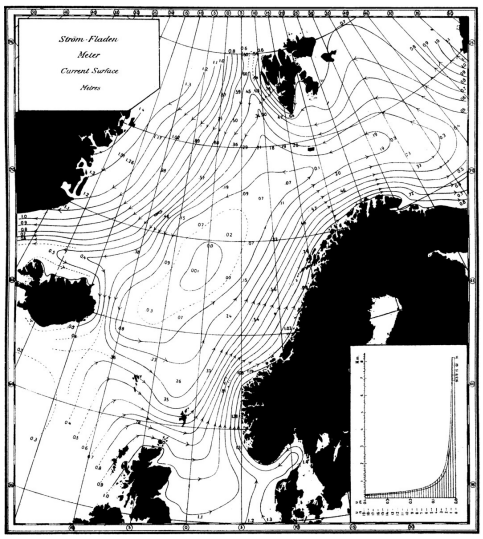

Figure 2.1: Current map by Henrik Mohn of the Norwegian Sea calculated by mean wind situation and internal distribution of water masses under the Norwegian North - Atlantic Expedition (Mohn 1878; Sætre 2007).

Figure 2.2: Current map of the Norwegian Sea by Bjørn Helland-Hansen and Fritjof Nansen presented in "The Norwegian Sea" in 1909 (Sætre 2012).

2.1.2 Norwegian Coastal Current (NCC)

The years 1900–1914 are considered as the golden years of the Norwegian marine research. Important persons in this period were Fritjof Nansen, Bjørn Helland-Hansen and Wilhelm Bjerknes. Nansen initiated and planned the physical oceanographic surveys in the Norwegian Sea with the research vessel "Michael Sars". Data surveys in the Norwegian Sea in the years 1900-1904 with "Michael Sars", supplemented with data from the Scottish and Danish oceanographers formed the basis for "The Norwegian Sea"', written by Helland-Hansen and Nansen in 1909 (Helland-Hansen and Nansen 1909; Sætre 2007). "The Norwegian Sea", presents results to calculate the currents at different depths by using density distribution combined with direct current measurements (Sætre 2012).

For the first time, observational material made it possible to analyze time series showing fluctuations in the Atlantic inflow into the Norwegian Sea. The results were compared to variations in atmospheric climate and ice conditions in the Barents Sea, and variations in heat transport into the Norwegian Sea. This gave the first general view of the Norwegian Coastal Current by Helland-Hansen and Nansen in 1909 (Sætre 2012). Figure 2.2 is a current map presented in "The Norwegian Sea" based on data from the expedition with "Michael Sars"from 1900-1904.

Two main water masses dominate along the Norwegian Coast, the Atlantic Water (SSS > 35) and the Norwegian Coastal water (SSS < 35). The distribution is shown in Figure

2.3. The inflow of Atlantic Water enters the Norwegian Sea and affects the Norwegian Coast through the Faroe Shetland Channel (Sætre and Ljøen 1972).

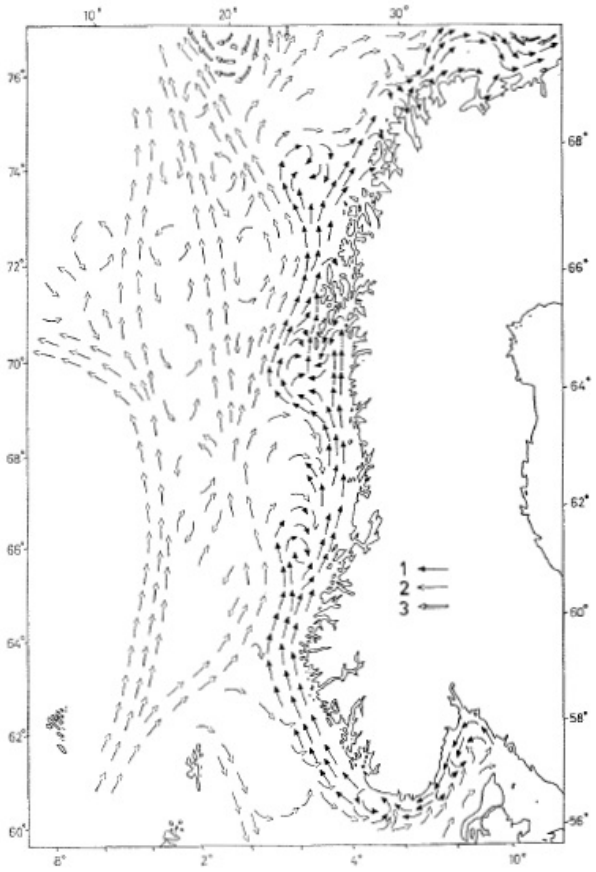

Figure 2.3: Distribution of water masses and current. 1) Coastal water, 2) Atlantic water, 3) Polar water (Sætre and Ljøen 1972).

The NCC has a clear seasonal profile. It has inclined boundary surface towards the surrounding water masses. Figure 2.4 illustrates how the light coastal water will spread out in a wedge form above the heavier underlying water (Sætre and Ljøen 1972). The wedge is deep, narrow during the winter, wide and shallow in the summer. The slope angle γ of the boundary surface can be expressed by the equation from Sætre and Ljøen (1972);

$$tan\gamma = \frac{f(\rho_2 v_2 - \rho_1 v_1)}{g(\rho_2 - \rho_1)} + \frac{\rho_2 v_2 - \rho_1 v_1}{Rg(\rho_2 - \rho_1)} \tag{2.1}$$

f: Coriolis parameter

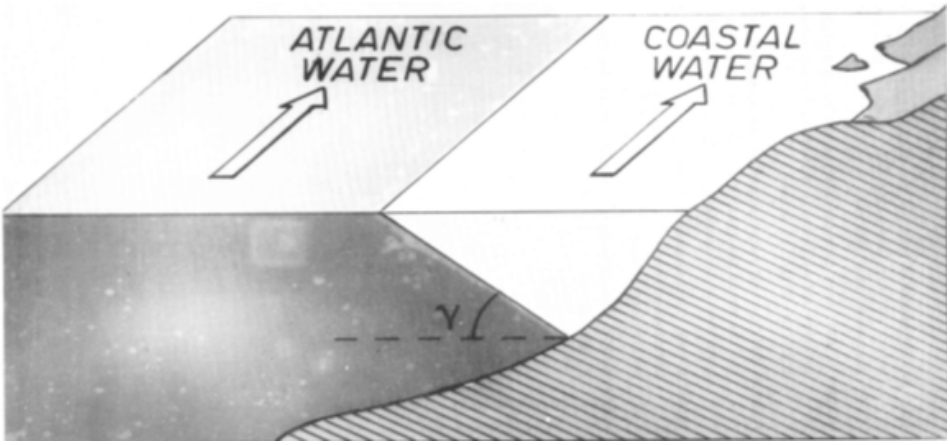

Figure 2.4: The light coastal water will spread out in a wedge form above heavier Atlantic water. The slope angle are expressed by Equation 2.1 (Sætre and Ljøen 1972).

g: Gravity constant

ρv: Density and velocity of the upper (1) and the lower level (2)

R: Radius of the curved trajectories

The last term of the equation can be omitted, if straight trajectories are assumed, and R will be infinity (Sætre and Ljøen 1972).

The Norwegian Coastal Current (NCC) is affected both locally and remotely by oceanic, atmospheric, bottom and terrestrial interactions. In Sætre (2007), there is a list of factors that influence movement and properties of the NCC, both long and short term, such as:

- Freshwater

- Tides

- Wind

- Atlantic water

- Bottom topography

The freshwater sources in the NCC are Baltic outflow (50%), freshwater runoff from Norway (40%) and freshwater runoff from the North Sea (10%) (Sætre 2007). The summer of 2014 in Scandinavia overall had higher temperatures than average (www.met.no/klima). This is likely to increase the fresh water runoff from Norway and may effect the oceanographic properties of the coastal water.

2.2 North Atlantic Current

The North Atlantic Current is a very important factor for the climate in Northern Europe with the supply of warm and salt water. This is an exchange of water between warm, saline water going northward (inflow) and cold, fresh water returning southward (overflow). When the warm, saline water reaches the Norwegian Sea it is cooled by the overlaying colder air and mixes with the water from the Arctic ocean (Hansen and Østerhus 2000). The water is cooled and when density increases, it sinks and forms an overflow returning southward. This process forces the warmer and saline water to higher latitudes. An important factor for its intensity is rising global temperature. A melting of the ice in polar areas will cause a fresher Arctic Ocean, and the northward inflow of the Atlantic Water will not be cooled and dense enough to cause a southward overflow. This may decrease the process of northward, warm and saline water, an important factor for the climate in North Europe (Sundby 2004). The main focus will from now on be on the inflow of Atlantic water between Iceland and Norway where the SailBuoy mission took place.

2.2.1 Greenland-Scotland Ridge

The Greenland-Scotland Ridge extends from Greenland to Scotland. It makes a barrier for the North-Atlantic - Nordic Sea exchange. The Nordic sea is a collective name for the Barents Sea, Greenland Sea, Iceland Sea and Norwegian Sea. In figure 2.5, the batymetry and surrounding water of the Greenland-Scotland Ridge are illustrated. The southward waters are separated in the surface overflow, near surface cold, fresh water returning near the Greenland coast and overflow, deep cold and dense water (Hansen and Østerhus 2000). The water exchange is very important for the global thermoline circulation for the climate of the Northern Europe (Sundby 2004). This is a region where a large number of expeditions have been carried out (Hansen and Østerhus 2000). Knudsen (1905) analyzed temperature and salinity from the mail streamer Laura from it's route from Denmark to Iceland via Faroe Island as early as in the years 1897–1904.

2.2.1.1 Topography

Iceland and the Faroe Islands are located in the Greenland-Scotland Ridge and divide the ridge into three gaps, Denmark Strait, Iceland - Faroe Ridge and Wyville - Thomson Ridge. Denmark Strait, between Greenland and Iceland has a sill depth of 620 m. The Iceland-Faroe Ridge, located between Iceland and the Faroe Islands is a wide ridge and has a minimum depth of 300-500 m near Iceland and deepening towards Faroe Island. The Wyville - Thomson Ridge has a depth of 600 m (Hansen and Østerhus 2000). This is

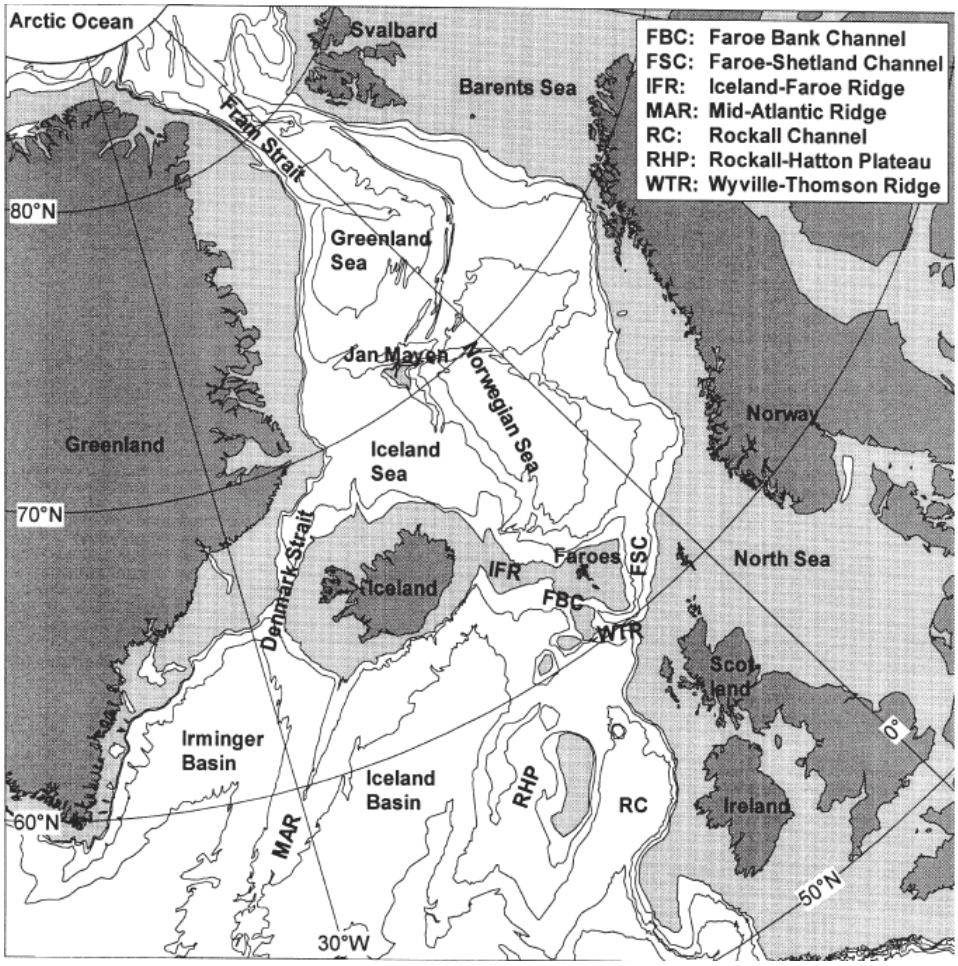

Figure 2.5: Bathymetry of the Greenland-Scotland region and surrounding waters. The light gray areas are illustrating areas shallower than 500 meter (Hansen and Østerhus 2000).

clearly shown in Figure 2.6. The Figure also include the broad and deep Faroe -Shetland channel, an important channel for Atlantic Water inflow to the Norwegian Sea, with a depth up to 840 m (Hansen and Østerhus 2000).

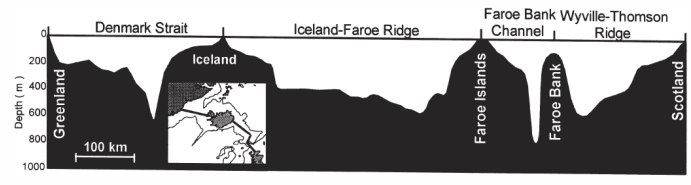

Figure 2.6: Bottom depth of the Greenland-Scotland Ridge (Hansen and Østerhus 2000).

2.2.1.2 Water masses

The effect of the inflow of Atlantic Water through the Greenland-Scotland ridge on the water masses in the Norwegian Sea is shown in Figure 2.7. This presents a vertical section crossing the Iceland - Faroe Ridge. On the Atlantic side of the ridge, the temperature and salinity are high (SST>5°C, SSS>35 psu) down to approximately 1000 m. Except close to the ridge where the temperature and salinity are lower. This is forced by the overflow of deep cold fresh water. On the other side of the ridge there are colder and less saline water masses. The Atlantic water that has crossed the ridge meets cold and low saline water and this forces the Iceland Faeoe Front. The Atlantic water has several gaps in the Greenland - Scotland Ridge to reach the Arctic Mediterranean, which contains the Arctic Ocean and the Nordic Sea. Figure 2.8 shows how the North Atlantic Current flows northward with warmer and more saline water near surface (Hansen and Østerhus 2000). Another characteristic water mass that may influence this mission is the arctic water going southward with the East Icelandic Current and its magnitude into the Iceland Sea.

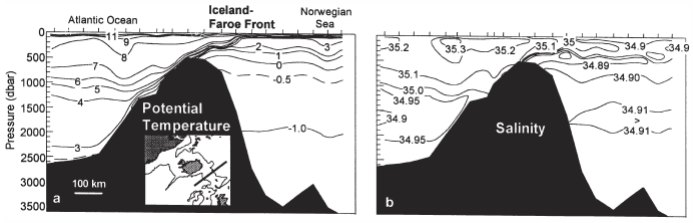

Figure 2.7: Potential temperature (a) and salinity (b) distribution crossing the Iceland-Faroe Ridge, from R/V Johan Hjort Nordic WOCE cruise 1994. Properties of the Atlantic Ocean and Norwegian Sea on each side of the ridge, and how it meets in the Iceland-Faroe Front (Hansen and Østerhus 2000).

Table 2.1: Typical properties of the main water mass exchange across the Greenland-Scotland Ridge (Hansen and Østerhus 2000).

Acronym	Name	Temperature range	Salinity range
MNAW	Modified North Atlantic Water	7.0 - 8.5°C	35.10 - 35.30
NAW	North Atlantic Water	9.5 - 10.5°C	35.35 - 35.45
MEIW	Modified East Icelandic Water	1.0 - 3°C	34.70 - 34.90
NSAIW	Norwegian Sea Arctic Intermediate Water	- 0.5 - 0.5°C	34.87 - 34.90
NSOW	Norwegian Sea Deep Water	< 0.5°C	34.91

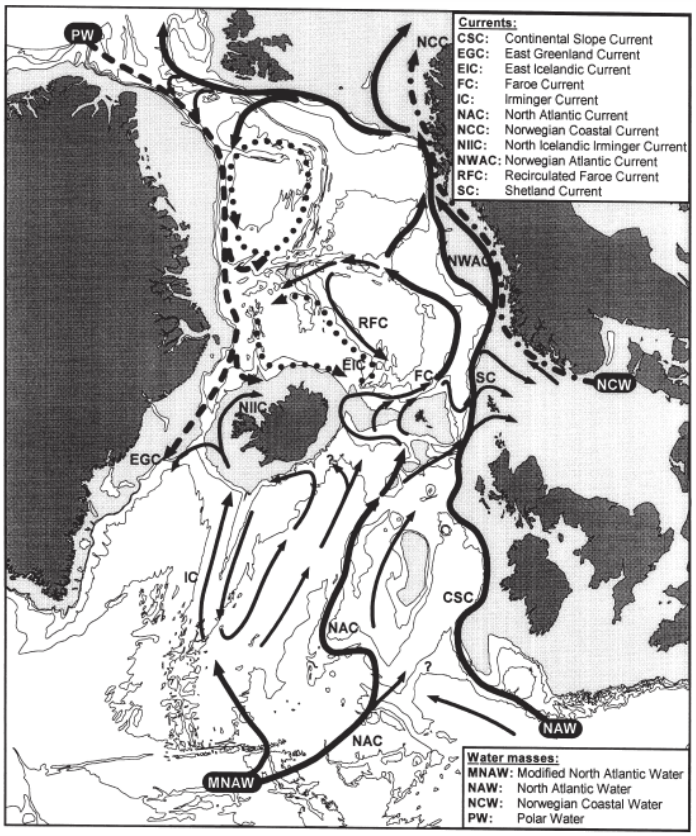

Figure 2.8: Near surface northward inflow of Atlantic water to the Arctic Mediterranean. Solid arrows show Atlantic water flow. Flows of other water masses are indicated with broken or dotted arrows (Hansen and Østerhus 2000).

Chapter 3

Instrumentation and measurements

3.1 Offshore Sensing SailBuoy

3.1.1 Technical description

The Offshore Sensing SailBuoy is an unmanned ocean vessel developed by Christian Michelsen Research (CMR) Instrumentation and now produced by Offshore Sensing (www.sailbuoy.no). It is a 100 % wind driven platform and it is capable of traveling the ocean for several months (Ghani et al. 2014). To power the on board electronics and actuators, batteries and solar panels are used. The power is used for navigation, power sensors, data loggers and communication. Power budgets are important issues for autonomous vessels (Peddie 2011). The SailBuoy is designed to use very little power, and the battery pack holds energy to navigate for 6 months without charging. It is not dependent on solar power for navigation, and this makes the SailBuoy more attractive for missions where solar power is limited. During navigation, the SailBuoy tracking to approach the way point the user has defined (Ghani et al. 2014).

The SailBuoy can measure both ocean and atmospheric parameters. It is designed to support a wide range of sensors and instrumentation on board. This makes it possible to use the SailBuoy for a wide variety of scientific and industrial applications. The SailBuoy can stay stationary or, as in this mission, travel from point to point (Fer and Peddie 2012).

The SailBuoy can both transmit data in real time via satellite and receive navigation instructions. The SailBuoy uses the Iridium Satellite system, which provides is a two-way communication (Fer and Peddie 2013). The technical specifications are listed in Table 3.1. An outline of the SailBuoy is presented in Figure 3.1.

Offshore Sensing SailBuoy	Technical descriptions
Length	2.0 m
Displacement	60 kg
Payload	15 kg / 60 l
Average speed	1-2 knots
Navigable wind speed range	2-20 m/s
Operational time	1 year
Communication	Iridium SBD
Payload solar power	20 W

Table 3.1: Technical description of the Offshore Sensing SailBuoy (Ghani et al. 2014).

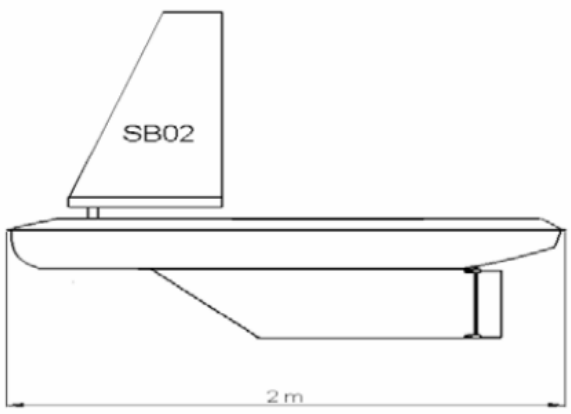

Figure 3.1: Outline of the Offshore Sensing SailBuoy (Ghani et al. 2014).

Number	**Date**	**Longitude** $[E/W]$	**Latitude** $[N]$
1	26.06.2014	4,88097	60,12531
2	30.06.2014	2,20404	60,21420
3	05.07.2014	-0,06255	61,47771
4	10.07.2014	-1,12722	62,43735
5	15.07.2014	-3,46299	63,17958
6	20.07.2014	-4,61007	62,94081
7	25.07.2014	-6,26466	63,01530
8	30.07.2014	-5,63466	62,71404
9	04.08.2014	-6,30750	63,50394
10	09.08.2014	-7,22931	64,33662
11	14.08.2014	-9,98061	63,64467

Table 3.2: Position of the Offshore Sensing SailBuoy during the field campaign in Figure 3.2.

3.2 Field campaign description

The SailBuoy was deployed outside the west coast of Norway(60.1391 N,4.8368 E) on 26 June 2014 and was recovered on 14 August 2014, after 49 days, outside Iceland (63.6360 N, 9.9477 W). Figure 3.2 shows the track of the SailBuoy together with marked positions with a 5 days interval, 12 UTC. It was equipped with a conductivity-temperature sensor (see section 3.3.1) and an oxygen optode (see section 3.3.2). The main goal of this mission was to investigate its performance in varying wind and current conditions. Since there were over 100 way points in this tracking period, it will not be focused on its performance due to navigation.

The sampling time for the data are varying. Within the three first days, from 26 June 2014, 7 UTC to 29 June 2014 7 UTC, the sampling rate varies between every 5., 10., 15., and 30. minutes. 279 of the total 1829 measurements, 15 %, are done within these days. From 28 June 2014 19 UTC, the sampling rate varies between every hour to every 30. minutes to the end of the campaign 14 August 2014 14.30 UTC. The SailBuoy was recovered by a Norwegian fishing vessel.

The weather conditions in summer 2014 was unusual with domination high pressure over Scandinavia. From March to August the mean temperature was 2.3 °C above normal (www.met.no/klima). Figure 1.2 present the air pressure for 25 June, 2 July, 11 July and 23 July 2014, illustrates a dominating high pressure over Scandinavian. The amount of precipitation were normal. With a higher average temperature, more freshwater sources may accouter along the Norwegian coast, and effect specially the coastal waters sea surface salinity.

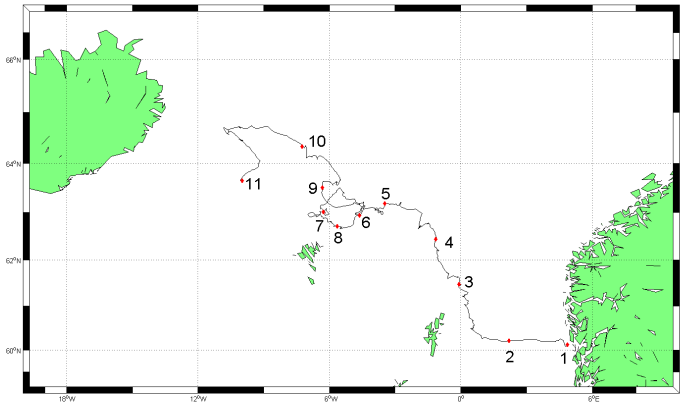

Figure 3.2: Track of the Offshore Sensing SailBuoy during the filed campaign. The positions marked by red, are buoy positions with a 5 day interval, see Table 3.2 for date and exact position coordinates.

3.3 Sensors

For this campaign, the SailBuoy was equipped with a Neil Brown conductivity-temperature sensor and an Aanderaa Instrumental oxygen optode.

3.3.1 Conductivity-temperature sensor

A glider CTD sensor designed by Neil Brown Ocean Sensors, Inc. (NBOSI) was equipped on the SailBuoy. The CTD sensor is a combination of a 4-electrode conductivity cell with an integral temperature sensor. This makes excellent dynamic response and high spatial resolution possible. The design is rugged and is resistant to fouling and is a low-drag, fast response unit. Since unmanned ocean vessels have limited space for batteries, it is important for the sensors to have low power consumption (Fer and Peddie 2013). To minimize impact on the vessel sailing performance, low drag of the sensors is desirable. A 4-electrode cells can be designed for rapid flushing, low thermal mass and low fluid-dynamic drag. The cell is shaped to avoid fouling by seaweed and other flotsam. The sensor was installed about 15 cm below water level, see Figure 3.3 (Ghani et al. 2014).

The sensor outputs data, as temperature and conductivity, are at a 5 Hz sample rate. DC power at 12 VDC is supplied to the CTD board. To generate the $\pm$ 5 VDC required by the board electronics, a DC/DC converter is used (Ghani et al. 2014). The board draws about 35 mA independent of the sample rate (Schmitt et al. 2006). The manufacturer

Figure 3.3: NBOSI G-CTD equipped on the Offshore Sensing SailBuoy (www.sailbuoy.no).

had calibrated the thermistor temperature sensor (Ghani et al. 2014).

Schmitt et al. (2006) compared temperature and salinity from the NBOSI G-CTD and a co-located Sea-Bird Scientific G-CT (SBE41). The results show that the NBOSI G-CTD is suitable for the SailBuoy (Ghani et al. 2014).

The salinity of seawater is defined by its electoral conductivity and calculated by following the Fofonoff and Millard (1983) approach. (See Appendix A).

3.3.2 Oxygen optode

It is important to measure the oxygen in the ocean since they are involved in most of the biological and chemical processes in the ocean (Ghani et al. 2014). In this campaign the AS4835, optode, manufactured by Aanderaa Data Instruments, Xylem Inc., was equipped on the SailBuoy. The optode has a diameter of 36 mm and a total length of 86 mm. It is made of Titanium and weighs 118 g. The output parameters are temperature in $°C$, dissolved oxygen concentration in μM and air saturation in %. It has a resolution of 0.01 C, 1 μM and 0.4 respectively (Aanderaa).

The optode is based on the ability of a selected substance to act as a dynamic fluorescence

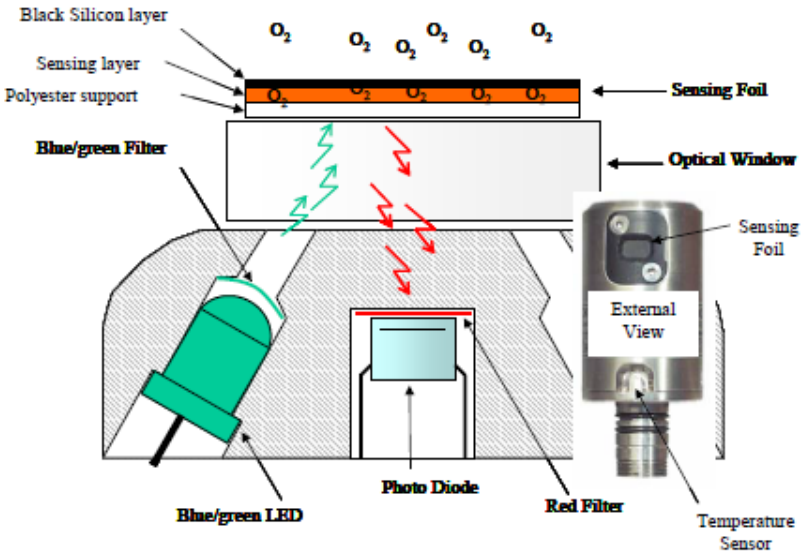

Figure 3.4: The principle behind oxygen optode. A blue light will be illuminated and the fluorescent indicator will emit a red light. The relationship between the oxygen concentration and the decay time of the emitted red light are described with Stern Volmer Equation 3.1 (Tengberg et al. 2006).

quencher and decrease fluorescence intensity or lifetime (Gytre 2004). The fluorescent indicator is a platinum porphyrin complex. This is illuminated with blue light, and emits red light back. The sensor will measure the decay time of the returning red light, which depends on the oxygen concentration in the ocean (Tengberg et al. 2006).

The relationship between oxygen concentration and the decay time of the emitted red light are described with Stern Volmer equation (Tengberg et al. 2006):

$$[O_2] = \frac{1}{K_{SV}}(\frac{\tau_0}{\tau} - 1) \tag{3.1}$$

where τ: Decay time.

τ_0: Decay time in the absence of oxygen

K_{SV}: Stern Volmer constant.

To protect from sunlight and fluorescent particles in the ocean, the complex is coated with a black optical isolation (Aanderaa).

3.4 Data processing

Data processing is an important part of this thesis. To be able to reproduce the result shown in this thesis, the data processes are described in this section.

A data reading routine has been programmed in Matlab to propose the data for further analysis. A control of the data is done to detect possible outliers, described in Section 6.1. The SailBuoy data has been interpolated into daily values (12 UTC) for the possibility to compare it with daily value data from ocean model simulations and remote sensing data. The velocity of the vessel is calculated from its displacement between known positions and time steps.

The data from ocean models, Forecast Ocean Assimilation Model 7 km Atlantic Margin Model (FOAM AMM7) and The Operational Mercator Global Ocean analysis and forecast system (MGO), and remote sensing data from Global Ocean Sea surface temperature and Sea Ice analysis (OSTIA), are obtained from www.myocean.eu.

3.4.1 Statistical methods

There are many ways to execute and present validation of models or remote sensing outputs. In this section a description of the statistical methods and errors that have been used to verify ocean model and remote sensing data are presented. To analyze the performance of the SailBuoy and verify remote sensing and ocean model data the correlation coefficient(r), the Mean Absolute Error (MAE) and the Mean Error (ME) are calculated.

3.4.1.1 Correlation coefficient (r)

The correlation coefficient (r) measures the magnitude of linear association between observations from the SailBuoy and remote sensing/model data.

$$r = \frac{cov(x, x_{SailBuoy})}{\sigma_x \sigma_{x_{SailBuoy}}} \tag{3.2}$$

where $cov(x, x_{SailBuoy})$ is the covariance, and σ the standard deviation. The correlation has a range of -1 $<$ r $<$ 1, where 0 indicate no linear correlation and $\pm$ 1 are perfectly correlated.

3.4.1.2 Mean Absolute error (MAE)

The Mean Absolute error (MAE) measures the magnitude of how close the model and remote sensing data is to reproduce the observations from the SailBuoy.

$$MAE = \frac{1}{n}\sum_{i=1}^{n}|(f_i - o_i)| \tag{3.3}$$

where f is the output from model/satellite, o is the observation from the SailBuoy and n is the number of time steps.

It ranges between 0 and ∞ and does not consider the direction of the error. The lower value, the better performance of the remote sensing or model.

3.4.1.3 Mean Error (ME)

The Mean Error (ME) is defined as

$$ME = \frac{1}{n}\sum_{i=1}^{n}(f_i - o_i) \tag{3.4}$$

where f is the output from model/remote sensing, o is the observation from the SailBuoy and n is the number of time steps.

ME indicates overestimate or underestimate of the models or remote sensing data. Positive values indicate overestimate, while negative values indicate underestimate. But it is important to remember that with a ME close to zero the model or remote sensing data does not necessarily have a perfect performance for all individual days. Individual errors may cancel each other out and bring the ME close to zero.

Chapter 4

Ocean models

The Offshore Sensing SailBuoy data has been compared with the models Forecast Ocean Assimilation Model 7 km Atlantic Margin Model (FOAM AMM7) and The Operational Mercator Global Ocean analysis and forecast system (MGO). Both models use the underlying model Nucleus for European Modelling of the Ocean, NEMO, but the data assimilation of satellite and in situ data are different (O'Dea et al. 2012; Lellouche et al. 2013).

The model data was obtained from www.myocean.eu. The MyOcean service has available ocean monitoring and forecasting.

4.1 Forecast Ocean Assimilation Model 7 km Atlantic Margin Model

The Forecast Ocean Assimilation Model 7 km Atlantic Margin Model (FOAM AMM7) is a hydrodynamic-ecosystem model and run by the UK Met Office. It is used to predict properties of the ocean, 3D daily mean fields of temperature, salinity and sea surface (zonal- and meridional) velocity and sea ice variables. It produces a daily analysis and a 5 days forecast. FOAM is the main UK input to the Global Ocean Data Assimilation Experiment (GODAE) (Martin et al. 2007). The model covers the European North-West continental Shelf (NWS) from 40°N, 20°W to 65°N, 13°E. The resolution of the model is 1/15° latitudinal resolution and 1/9° longitudinal resolution. This gives approximately a horizontal resolution of 7 km (O'Dea et al. 2012). The FOAM system is based upon Nucleus for European Modelling of the Ocean (NEMO) code version 3.4 described in Madec (2012). For the assimilation of the sea surface temperature the

model uses a version of NEMOVAR described in Mogensen et al. (2012) (O'Dea et al. 2012).

4.1.1 Nucleus for European Modelling of the Ocean (NEMO)

Nucleus for European Modelling of the Ocean, NEMO, is a primitive equation model and is used for studying ocean circulations and its impact on the earth's climate system (Madec 2012).

4.1.1.1 Primitive equations

The hydrodynamic model is based on the primitive equations i.e. the Navier-Stokes equations along with nonlinear equations of state. It is chosen to use a orthogonal set of unit vectors (i,j,k). By following the Madec (2012), the primitive equations are:

The momentum balance:

$$\frac{\delta U_h}{\delta t} = -[(\nabla \times U) \times U + \frac{1}{2}\nabla(U^2)]_H - f\mathbf{k} \times U_H - \frac{1}{c}\nabla_H P + D^U + F^U \tag{4.1}$$

The hydrostatic equilibrium:

$$\frac{\delta p}{\delta z} = -\rho g \tag{4.2}$$

The incompressibility equation:

$$\nabla \bullet \mathbf{U} = 0 \tag{4.3}$$

The heat and salt conservation equation:

$$\frac{\delta T}{\delta t} = -\nabla \bullet \ (T\mathbf{U}) + D^T + F^T \tag{4.4}$$

$$\frac{\delta S}{\delta t} = -\nabla \bullet \ (S\mathbf{U}) + D^S + F^S \tag{4.5}$$

Equation of state:

$$\rho = \rho(T, S, P) \tag{4.6}$$

The variables are defined as

U = Uh + w k, velocity vector where h denotes the local horizontal vector,

S: salinity,

T: potential temperature,

g: gravity

ρ: in situ density.

ρ_0: reference density

p: pressure

f = $2\Omega \cdot k$: Coriolis term

DU, DT, DS: parametrization of small-scale physics for momentum, temperature and salinity

FU, FT, FS: surface forcing terms.

The model is also based upon six assumptions from Madec (2012).

(1) Spherical earth approximation: The geopotential surfaces are assumed to be spheres so that gravity (local vertical) is parallel to the radius of the earth.

(2) Thin-shell approximation: The ocean depth is neglected compared to the radius of the earth.

(3) Turbulent closure hypothesis: The turbulent fluxes (which represent the effect of small scale processes on the large-scale) are expressed in terms of large scale features.

(4) Boussinesq hypothesis: Density variations are neglected except in their contribution to the buoyancy force.

(5) Hydrostatic hypothesis: The vertical momentum equation is reduced to a balance between the vertical pressure gradient and the buoyancy force.

(6) Incompressibility hypothesis: The three dimensional divergence of the velocity vector is assumed to be zero.

4.1.1.2 Boundary conditions

The ocean has two boundaries, coastlines including the bottom topography boundary, and air-sea or ice-sea boundary. This makes it bounded by two surfaces z = - H(i,j) and z = η(i,j,t). Through these two boundaries, the ocean can exchange fluxes of heat, salt,

fresh water and momentum. These are all factors that affect ocean properties. In the interface between land and ocean, the major flux exchange is fresh water. This is through river runoff and affects the sea surface salinity. Between the solid earth and ocean, the momentum flux is the most important. Heat and salt fluxes through the sea bed are relatively small and usually neglected in the model. Exchange between the atmosphere and the ocean is horizontal momentum, as wind stress, heat and mass exchange of fresh water. The fresh water flux is a budget of precipitation minus evaporation. The last interface is between the ocean and sea ice where heat, salt, fresh water and momentum fluxes are exchanged (Madec 2012).

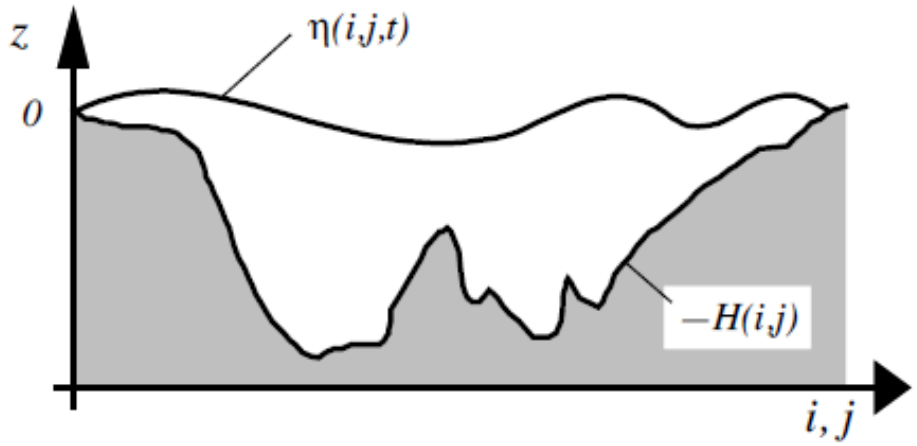

Figure 4.1: Boundary conditions in Nucleus for European Modelling of the Ocean(NEMO). Illustrates the boundaries of the ocean. z= - H(i,j) and z = η(i,j,t), where H is the depth of the ocean, and η is the sea surface elevation (Madec 2012).

4.1.1.3 Time stepping

The model time stepping environment is a three level scheme in which the tendency term of the equation is evaluated whether centered in time, or forward, or backward in time depending of the nature of the term (Madec 2012).

4.1.1.4 Spatial discretization

To solve the primitive equations in models we need numerical techniques. The NEMO uses a staggered Arakawa C grid in the horizontal direction, described in Arakawa and Lamb (1981)(Madec 2012). By using this type of grid, the variables or tracers,

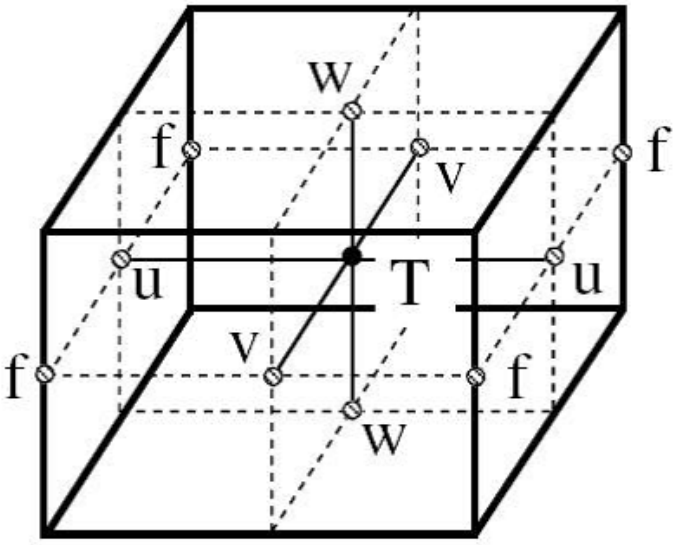

Figure 4.2: Spatial discretization in NEMO. Arakawa C grid where T indicates grid point where temperature, salinity, density, pressure and horizontal divergence is defined in the center of the grid cell. The velocity (u,v,w) are located in the mid-point between grid cells and therefore one-half grid from the tracker point (Madec 2012).

as temperature, salinity, density, pressure and horizontal divergence are defined in the center of the grid cell, see Figure 4.2. The velocity (u,v,w) are located in the mid-point between grid cells and therefore one-half grid from the tracker point. All the products from the model have been delivered from the tracker grid. Since the velocity variables are located one-half from the tracker point it has to be interpolated from its actual position (Madec 2012).

4.1.2 Data assimilation

The scheme used for data assimilation for SST in FOAM AMM7 are NEMOVAR data assimilation scheme (Blockley et al. 2013). Earlier the FOAM AMM7 used the Analyze Correction method, described by Martin et al. (2007). The data assimilation can be written as a three step (O'Dea et al. 2012). The first step is a one day model run and is compared by using the First Guess at Approriate Time (FGAT) system. Here a one day model forecast is compared with observations at the nearest time step. In the second step observations minus model difference is done by minimizing the cost function described in Mogensen et al. (2012). A special mechanism by NEMOVAR is how it uses correlation between ocean variables to write ocean parameters as a sum of balance and

unbalance components. In the final stage the model uses Incremental Analysis Update (IAU) described in Bloom et al. (1996)

The data assimilation are done by using in-situ data from the Global Telecommunication System (GTS) and satellite data from Group for high resolution Sea Surface temperature, GHRSST. The satellite data includes SST data from the SEVIRI instrument on the Metosat geostationary satellite and from the AVHRR instrument on the NOAA and METOP satellite (Blockley et al. 2013).

4.2 The Operational Mercator global Ocean analysis and forecast system

The Mercator Ocean monitoring and forecasting system has been responsible for the global ocean forecasting in the MyOcean project for a long time. It is a global product (180° W- 180° E; 77° S - 90° N) and produces a 3D daily mean potential temperature, salinity and current information from the top to the bottom global ocean. It also has a 2D sea surface level, sea ice thickness, sea ice fraction and sea ice velocity. By using several configurations it may cover different geographical areas with various vertical and horizontal resolutions. It is a global high-resolution model with 1/12° horizontal grid spacing and 50 vertical levels (Lellouche et al. 2013).

The Mercator Ocean Global Ocean 1/12° forecasting system uses the NEMO 3.1 (Nucleus for European Models of the Ocean) modeling system. NEMO 3.1 is based on the same primitive equations, boundary conditions, time and spatial discretizations as in FOAM AMM7, see Section 4.4.1, described by Madec (2012). The data assimilation in MGO system is using surface field forcing of the ocean from European Center for Medium Range Weather Forecast (ECMWF), satellite data (NOAA/AVHRR, ENVISAT,MGS,TMRR) and in-situ observations (drifting buoys, ships) available via CORIOLIS (http://www.coriolis.eu.org/) (Lellouche et al. 2013).

4.2.1 Data assimilation

The Mercator Ocean Global Ocean 1/12° forecasting system uses the SAM-2 (Système dAssimilation Mercator) data assimilation system. The SAM method relies on a reduced order Kalmar filter (Lellouche et al. 2013). This is based on a formulation introduced by Pham et al. (1998), the singular evaluative extended Kalman filter, SEEK (Lellouche et al. 2013). The data assimilation is produced by using in-situ data from CORIOLIS and satellite data. The satellite data includes SST data from NOAA/AVHRR,

ENVISAT,MGS,TMRR. In addition to the assimilation scheme a bias correction (3D VAR) with Incremental Analysis Update (IAU) is used (Lellouche et al. 2013).

Chapter 5

Remote sensing

Daily sea surface temperature data from the Offshore Sensing SailBuoy have been compared with The operational sea surface temperature and sea ice analysis (OSTIA) system. The OSTIA data are obtained from www.myocean.eu. Sea surface salinity measured by remote sensing is still limited, but the SSS data from the SailBuoy and the SSS data from the Aquarius Instrument is discussed in Chapter 7.

5.1 The operational sea surface temperature and sea ice analysis system

The operational sea surface temperature and sea ice analysis system, OSTIA, use satellite data provided by the Group for high resolution Sea Surface temperature, GHRSST, project together with in-situ observations, to determine the SST (Stark et al. 2007).

The operational sea surface temperature and sea ice analysis system (OSTIA) is run by the UK Met Office. To determine the SST, the OSTIA uses a combination of data from a satellite provided by GHRSST together with in-situ data from ships, drifters and moored buoys. The in-situ data are available over the Global Telecommunications system (GTS). The product from GHRSST includes data from both infrared- and microwave satellite instruments. The satellite used for SST data in OSTIA is: infra-red data from the AVHRR instruments on board NOAA and MetOp-A satellites, IASI data on MetOp-A, SEVIRI on board the MSG-2 satellite, GOES Imager data on board the GOES-13 satellite and microwave data from the TMI instrument on board TRMM (Donlon et al. 2012). All data sources are presented in Table 5.1.

The satellite data from infrared space instruments has a nadir spatial resolution of 1

km and a high accuracy of $\sim 0.3 - 0.6K$. Measurements of SST can be done by passive microwave radar, by using the 6-10 GHz band. The roughness of the ocean makes a change in the brightness temperature. The brightness temperature is measured by using information in both horizontal and vertical polarizations. By using the 6-10 GHz bank, the microwave radiation will not have problems with clouds, atmospheric water vapor and aerosols (Donlon et al. 2012).

5.1.1 Data analysis

All satellite data of sea surface temperature are aligned for daily bias error and filtered to remove diurnal variability. It can be biased by atmospheric water vapor and aerosols, surface changes as extreme roughness and problems with the instrumental calibration. This is done by a statistic match up of the satellite data and reference measurements (in situ data and a high quality subset of the MetOp AVHRR satellite data).

The background of the analyzed SST is done based on previous days analysis together with climatology defined by following Donlon et al. (2012) as:

$$x^b_{i,k} = \lambda_{i,k}(x^a_{i,k-1} - x^c_{i,k-1}) + x^c_{i,k} \tag{5.1}$$

$x^b_{i,k}$: Background field

$\lambda_{i,k}$: Scalar less than 1

$x^a_{i,k-1}$: Previous analysis

$x^c_{i,k-1}$: Climatology value for the same time as the previous analysis

$x^c_{i,k}$: Climatology for the new analysis time

To combine the bias corrected measurements and the results from Equation 5.1, the system uses a multiscale optimal interpolation described in Martin et al. (2007) to produce an analysis (Donlon et al. 2012).

Table 5.1: Data sources and its characteristics used in The operational sea surface temperature and sea ice analysis (OSTIA) system. OSTIA uses in-situ and satellite data from both infrared and microwave radiometers (Stark et al. 2007).

Sensor	**Sensor Type**	**Resolution**	**Data source**	**Coverage**	**Subsamling**
AATSR (EnviSat)	Infra-red	1km (swath)	ESA-Medspiration	Global (1.5×10^6)	3x3
AMSR-E (Aqua)	Microwave	25km (swath)	Remote Sensing Systems	Global (6×10^5)	2x2
AVHRR-LAC (NOAA 17 and 18)	Infra-red	$1/10^\circ$	ESA-Medspiration	North-East Atlantic and Mediterranean (1×10^4)	3x3
AVHRR-GAC (NOAA 18)	Infra-red	9km (swath)	JPL PO-DAAC	Global (8×10^5)	None
In situ temperature and salinity	Ships, drifting and moored buoys.	In situ	Global Telecommunications System (GTS)	Global (4×10^4)	None
Sea Ice, primarily SSM/I (DMSP)	Microwave	10km (Polar-stereographic grid)	EUMETSAT OSI-SAF	Global	None
SEVERI (MSG1)	Infra-red	0.1°	ESA-Medspiration	Atlantic sector (6×10^4)	None
TMI (TRMM)	Microwave	25km (swath)	Remote Sensing System	Tropics (5×10^4)	2x2

5.2 Aquarius Instrument

To compare the sea surface salinity data from the SailBuoy with a satellite product, we used a product from Aquarius Instrument developed under NASA's Earth system Science Pathfinder (ESSP) program. Aquarius Instrument is a combination radiometer and scatterometer designed to map the sea surface salinity. It is a combined active/passive microwave instrument operation at L-band, 1.413 GHz for radiometer and 1.26 GHz for scatterometer (Le Vine et al. 2007). It has a spatial resolution of 150 km and an accuracy of $\sim$ 0.2 psu (Le Vine et al. 2006). To measure SSS remotely, it use a passive microwave sensor, the radiometer. The change of salinity changes the conductivity of the ocean. This affects the microwave emissivity from the seawater. It is measured to cause a change of 0.5 K/psu at L-band and modern microwave radiometers can measure it in microwave frequency 1.4 GHz (Le Vine et al. 2010).

5.2.1 Measurement physics

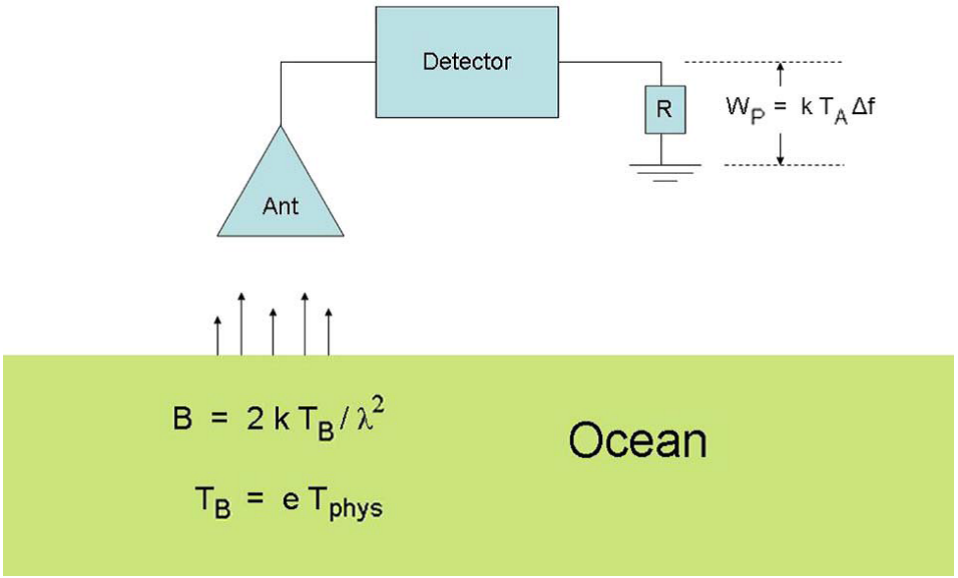

Figure 5.1: The physical behind measurements from remote sensing. The radiation is collected by the antenna and amplified in the receiver. Wp is the expression of the output energy at polarization p (Le Vine et al. 2010).

Salinity changes the microwave emissivity. Information given here is from Le Vine et al. (2010). If a "blackbody" is assumed, the thermal radiation emitted from the source, is given by Rayleigh's Jean law:

$$B(f) = 2kT_{phys}/\lambda^2 \tag{5.2}$$

Where k is the Boltzmann's constant, T_{phys} is the physical temperature, $\lambda = c/f$ is the wavelength and f is the frequency.

Since the ocean can not be seen a "blackbody", the physical temperature changes by brightness temperature $T_B(\Omega, f)$:

$$T_B(f) = e(f)T_{phys} \tag{5.3}$$

Where $e(f)$ is emissivity. The emissivity is a quantity that depends on factors as salinity and temperature, but also waves/roughness of the ocean, the incident angle, frequency and polarization. As shown in Figure 5.1, the emissivity is measured by the microwave radiometer.

By changing the physical temperature with the brightness temperature we get a new equation for brightness B(f):

$$B(f) = 2kT_B/\lambda^2 \tag{5.4}$$

Figure 5.2 illustrated the principle of Aquarius. The radiometer is looking down from its orbit towards the ocean. It measure the thermal emission from the surface (black solid line in Figure 5.2). To combined it with knowledge sea surface temperature, it estimate the sea surface salinity (Le Vine et al. 2010).

Factors that may complicate the remote sensing of salinity are such as waves on the ocean. It makes a change in the surface roughness and this causes a change in the observed brightness temperature. This is the reason why the Aquarius Instrument includes both a radiometer and a scatterometer. To make the measurements as accurate as possible the radiometer and the scatterometer operate nearly at the same frequency (radiometer 1.413 GHz, scatterometer 1.26 GHz). It is important that they share the same antenna feed to make it possible to look at the same pixel with the same footprint (Le Vine et al. 2010).

Another source of error that has to be taken into account is the Faraday rotation. As the radiation propagates from the surface to be picked up by the sensor, it will make a rotation of the polarization trough the ionosphere when it arrives at the sensor. Since the emissivity depends on the polarization, it will change the brightness temperature and make it a possible error source. Therefore, a polarimetric channel supplies the radiometer in Aquarius Instrument. This uses the third Stokes parameter (correlation

between horizontal and vertical polarizationion) and an algorithm suggested by Yueh (2000) (Le Vine et al. 2010).

Another source of error on the radiation in L-band is the sun. To avoid reflection from the ocean surface and to minimize the radiation from the sun, the Aquarius instrument antenna is pointed away from the sun, towards the nighttime side of the ground track, see Figure 5.3 (Le Vine et al. 2010; Le Vine et al. 2005).

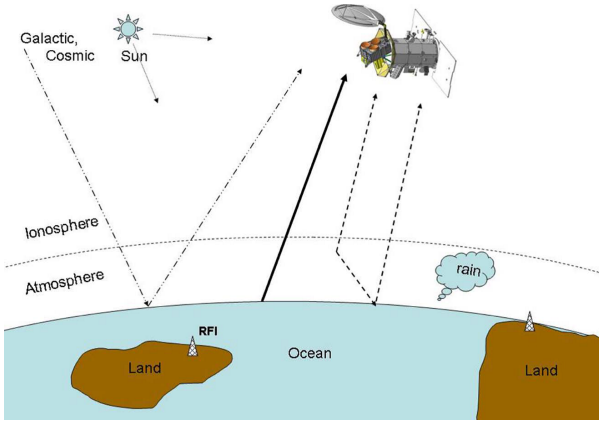

Figure 5.2: Illustrates possible error sources of radiation when remote sensing sea surface salinity at L-band (Le Vine et al. 2010).

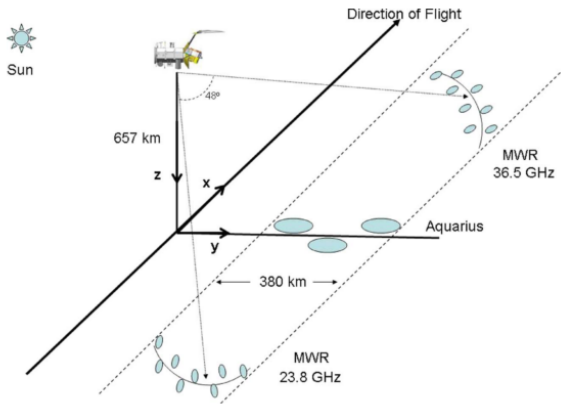

Figure 5.3: The Aquarius Instrument is pointed to the nighttime side of the ground track. The Microwave Radiometer are covering the same swath as the Aquarius Instrument (Le Vine et al. 2010).

The present of land is another source of error on remote sensing of salinity from space. Land is radiomatrically much warmer than ocean, so a small amount of land in the measured footprint can error the salinity calculation. This make the salinity measured

from space difficult, and near the coast, the salinity measurements have reduced accuracy (Le Vine et al. 2010).

Chapter 6

Results

6.1 The Offshore Sensing SailBuoy measurements

The Offshore Sensing SailBuoy campaign was carried out from 26 June 2014 to 14 August 2014. The SailBuoy was deployed outside the west coast of Norway(60.1391 N,4.8368 E) was recovered after 49 days, outside Iceland (63.6360 N, 9.9477 W). The sampling time for the data are varying. Within the three first days, from 26 June 2014, 7 UTC to 29 June 2014 7 UTC, the sampling rate varies between every 5., 10., 15., and 30. minutes. 279 of the total 1829 measurements, 15 %, are done within these days. From 28 June 2014 19 UTC, the sampling rate varies between every hour to every 30. minutes to the end of the campaign 14. August 2014 14.30 UTC. The SailBuoy was recovered by a Norwegian fishing vessel. Figure 6.1 shows the track of the SailBuoy in combination with velocity vectors. The velocity is deduced from its displacement between known positions and known time steps. The average speed and standard deviation was $74cm^{-1}$ and $56cm^{-1}$. It had a maximum speed of $314.6cm^{-1}$ the 10 August 2014, when the SailBuoy was located in the region between Iceland and the Faroe Island.

A quality control of the data was undertaken in order to detect outliers with a numerical distance from the remaining data. A scatter plot of conductivity against temperature can be made to locate possible outliers by linear regression. The SailBuoy started at the Norwegian coast, the coastal water has a low sea surface salinity that will affect the conductivity. Conductivity is strongly dependent of temperature, but only if salinity contributions are negligible. A Temperature - Salinity diagram for all 1829 data points is presented in Figure 6.2a. One obvious outlier with salinity ~ 0.3 psu is detected. The bias may be due to the recovery of the SailBuoy as this was data point number 1829 and is from now on deleted. Figure 6.2b illustrates a Temperature - Salinity diagram divided into three time periods with water masses of different characteristics along the mission.

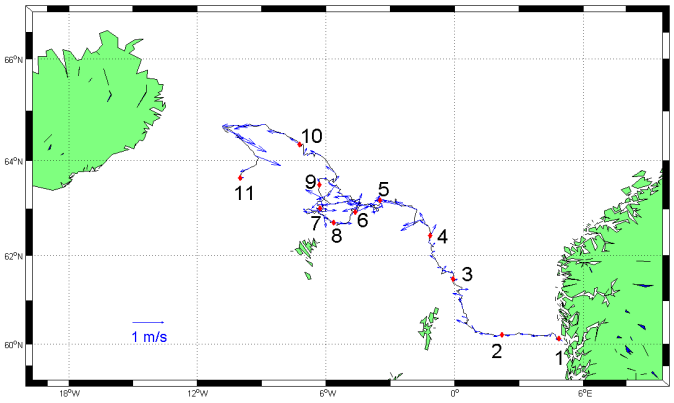

Figure 6.1: Track of the Offshore Sensing SailBuoy together with velocity vectors. See Table 3.2 for the positions marked in red.

The red are coastal water with typical salinity of 30.3–31.1 psu near the Norwegian coast from 26.06.2014 7.11 UTC to 29.06.2014 10 UTC. These are data points 1 to 285. The green scatter presents when the SailBuoy was affected by Atlantic Water and coastal water from 29.06.2014 10 UTC to 02.07.2014 11 UTC, data point 286 to 430. The blue points are when Atlantic Water dominated and the salinity is stabilized around 35 psu from 02.07.2014 11 UTC to 14.08.2014 14 UTC, data points 431 to 1828.

A Temperature - Salinity diagram is made for the area near the Norwegian coast. (The red points in Figure 6.2b.) Figure 6.3a presents these 285 first data points together with a black regression line. An outlier is defined as points further than 3 standard derivations away from the regression line, marked by blue lines in Figure 6.3a. No outliers were detected here. The scatter plot of temperature against conductivity for the region when the salinity is stabilized around 35 psu, data points 430 to 1828, is presented in Figure 6.3b. Two outliers were detected and replaced by linear interpolation. The two outliers are marked with a black circle in Figure 6.3b.

Sea surface temperature, salinity and dissolved oxygen concentration measured by the SailBuoy along the track is shown in Figure 6.4. The measured values are between $8.5 - 14.6°C$ for temperature, $30.3 - 35.3$ psu for salinity and $8.6 - 10$ mg/l for O_2 concentration. The clear difference in temperature, salinity and oxygen at the beginning of the campaign shows the region where the Norwegian coastal water is dominant. The temperature is high, oxygen and salinity are low.

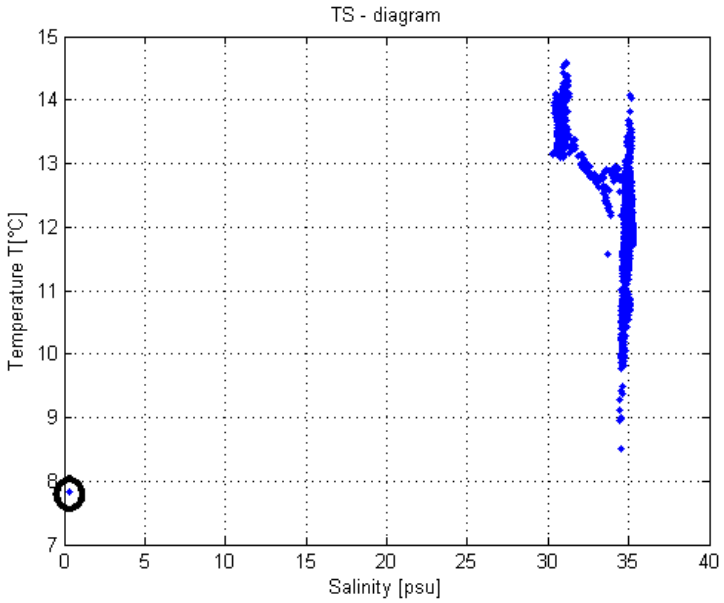

(a) Temperature - Salinity diagram to detect outliers of the 1829 data points from the Offshore Sensing SailBuoy. One outlier are detected and marked by a black circle.

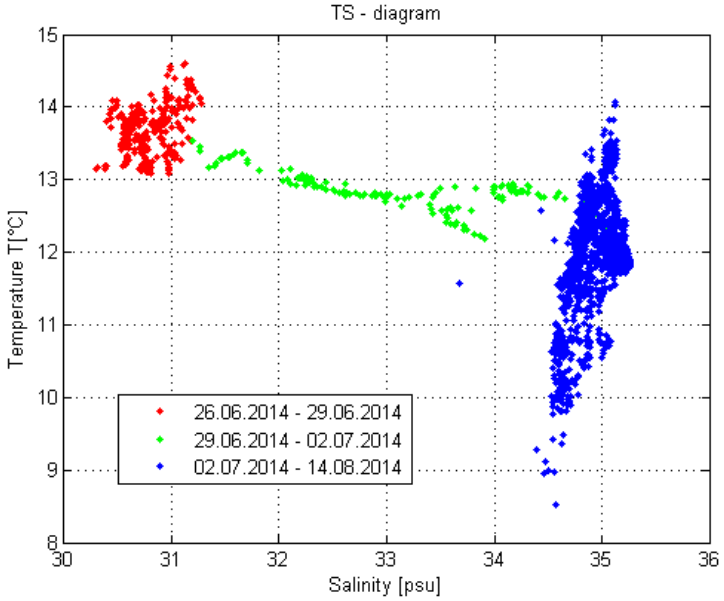

(b) Temperature - Salinity diagram. Three time periods with water masses of different characteristics. Red dots: the Offshore Sensing SailBuoy is outside the western coast of Norway from 26.06.2014 7.11 UTC to 26.06.2014 10 UTC. Green dots: The Offshore Sensing SailBuoy are leaving the coast and affected by Atlantic Water on the way, 29.06.2014 10 UTC to 02.07.2014 11 UTC. Blue dots: Atlantic Water is dominating, salinity is stabilized around 35 psu, from 02.07.2014 11 UTC to 14.08.2014 14 UTC.

Figure 6.2: Temperature - Salinity diagrams to detect outliers from the Offshore Sensing SailBuoy data.

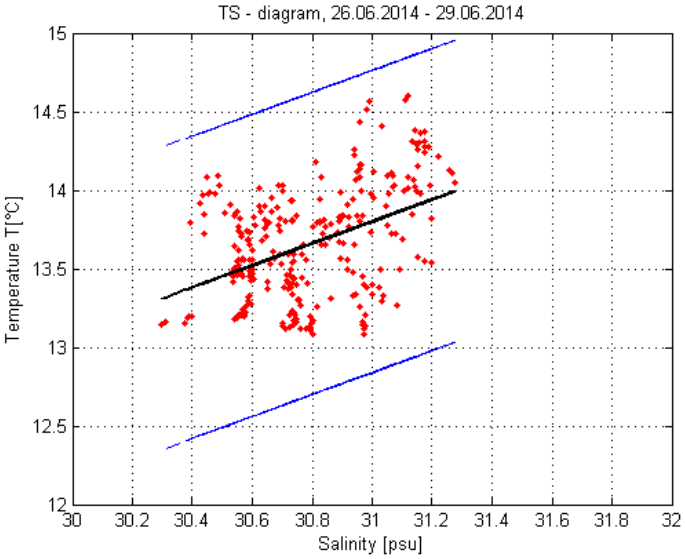

(a) A Temperature - Salinity diagram of the Offshore Sensing SailBuoys temperature and salinity data from 26.06.2014 7.11 UTC to 29.06.2014 10 UTC, 285 data points together with a black regression line. An outlier is defined as values further than 3 standard deviation away from the regression line, blue lines. No outliers are detected here.

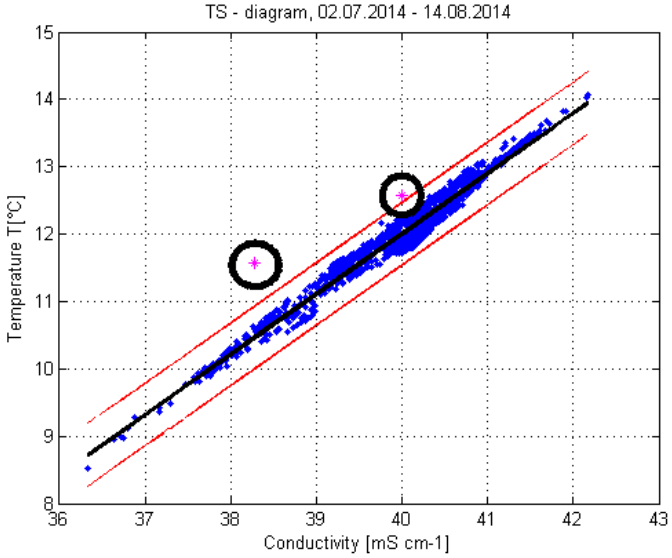

(b) Scatterplot of temperature against conductivity from the Offshore Sensing SailBuoy collected data from 02.07.2014 11 UTC to 14.08.2014 14 UTC. Data point number 430 to 1828 together with a black regression line. An outlier is defined as values further than 3 standard deviation away from the regression line, red lines. Two outliers are detected here, marked with black circles.

Figure 6.3: Quality control of the Offshore Sensing SailBuoy measurements, detect outliers.

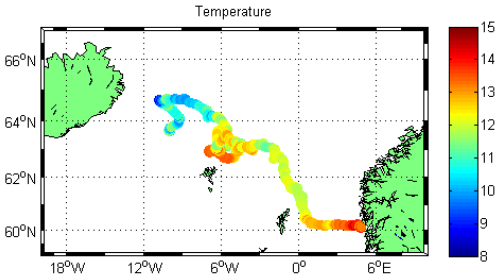

(a) Track of the Offshore Sensing SailBuoy. The colour indicate temperature [°C].

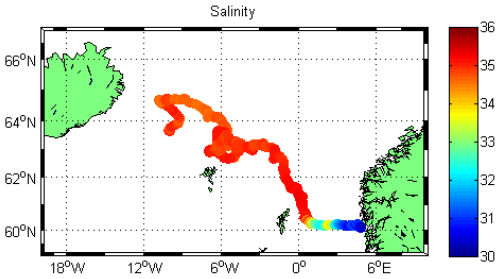

(b) Track of the Offshore Sensing SailBuoy. The colour indicate salinity [psu].

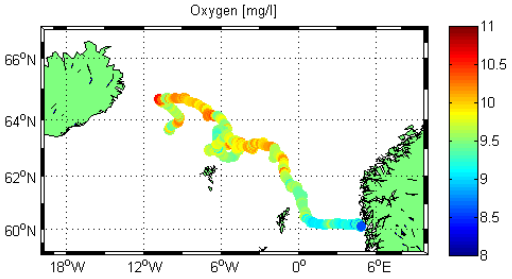

(c) Track of the Offshore Sensing SailBuoy. The colour indicate dissolved oxygen concentration [mgl^{-1}].

Figure 6.4: Maps with the Offshore Sensing SailBuoy track showing (a) temperature [°C], (b) salinity [psu] and (c) dissolved oxygen concentration [mgl^{-1}].

Time series of temperature, salinity and conductivity are presented in Figure 6.5. The red trackers are the full resolution data and the black trackers present the daily mean time series. The measured SST varies between 8.5 and 14.6 $°C$. The maximum value occurs when the SailBuoy is in coastal region outside the western Norwegian coast, 28 June 2014. The calculated salinity varies between 30.3 and 35.3 psu. The transition from coastal and river-influence/freshwater region to offshore more saline water is evident. The salinity value increases until about 02 July 2014 and the salinity stabilizes around a value of 35 psu.

Figure 6.6 shows O_2 air saturation and O_2 concentration. There is a clearly diurnal variation, which is a result of the production of oxygen during photosynthesis and loss during respiration and decompositions. The photosynthesis needs light and therefore the production of oxygen due to photosynthesis happends in daylight. The loss of oxygen due to breakdown of organic matter by bacteria and fungi, is not dependent of light, and may occur all 24 hours a day. The oxygen concentration values are between $8.5 - 10.6 mgl^{-1}$. The maximum value of dissolved oxygen concentration occurs at the same time as the minimum value of temperature. This is because cold water and less saline water can hold more gas than warm and more saline water.

Time series of temperatures measured by the NBOSI sensor and the temperature sensor on the oxygen optode AS4835 are shown in figure 6.7. The AS4835 optode has a diurnal variation, but the daily mean shows a good correlation of temperature measurements. Both of the sensors have the same maximum temperature in the beginning of the campaign, 28 July 2014, and the significant drop in the end, around 10 August 2014. This shows that maxima and minima in temperature not are due to erroneous measurements, but do to changes in water masses and fronts. For SST comparison and validation of model simulations and remote sensing data, data from NBOSI sensor are used.

6.2 Offshore Sensing SailBuoy data compared with ocean model simulations

The SailBuoy data were compared with two models, Forecast Ocean Assimilation Model 7 km Atlantic Margin Model (FOAM AMM7) and The Operational Mercator Global Ocean analysis and forecast system (MGO).

Daily averaged data of sea surface temperature and sea surface salinity from the SailBuoy are compared with daily average data from FOAM AMM7 and MGO. In this thesis, the positions from ocean models and remote sensing are chosen by finding the nearest grid point to the average daily position of the SailBuoy. See appendix B for values of SST, SSS, positons coordinates for FOAM AMM7, MGO and SailBuoy.

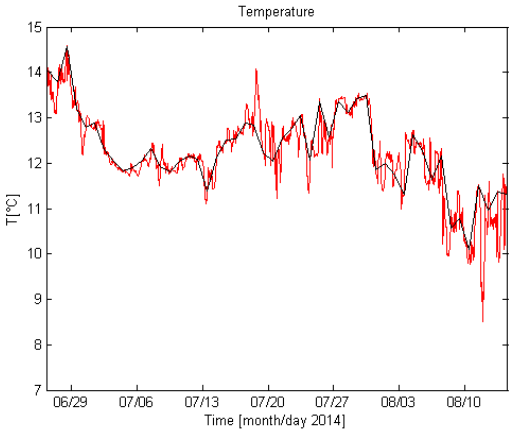

(a) Time series of temperature.

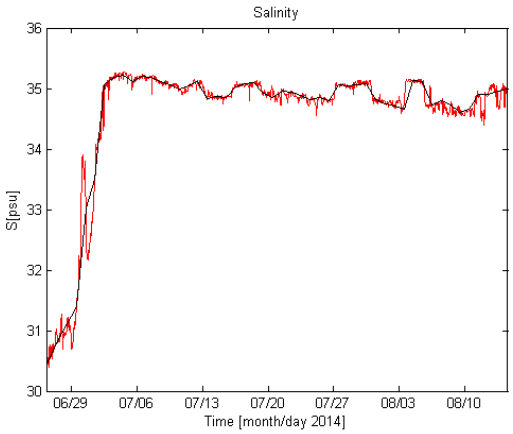

(b) Time series of salinity.

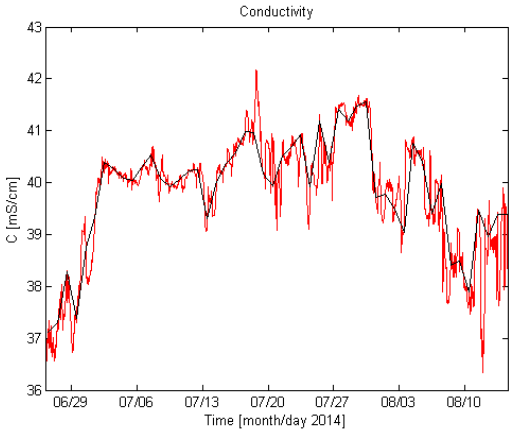

(c) Time series of conductivity.

Figure 6.5: Time series of (a) temperature [°C], (b) salinity [psu], and (c) conductivity [mg/l] from the Offshore Sensing SailBuoy. The red trackers are the full resolution data and the black trackers illustrates the daily mean time series.

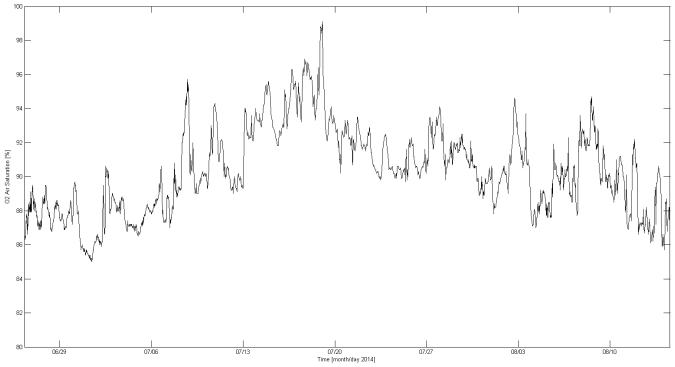

(a) Time series of oxygen air saturation

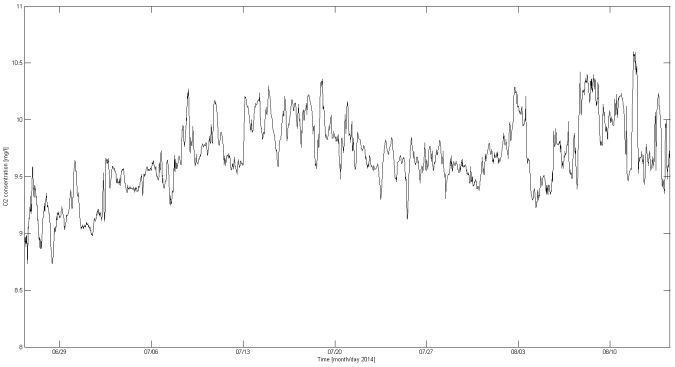

(b) Time series of dissolved oxygen concentration.

Figure 6.6: Time series of (a) oxygen air saturation and (b) dissolved oxygen concentration from the Offshore Sensing SailBuoy.

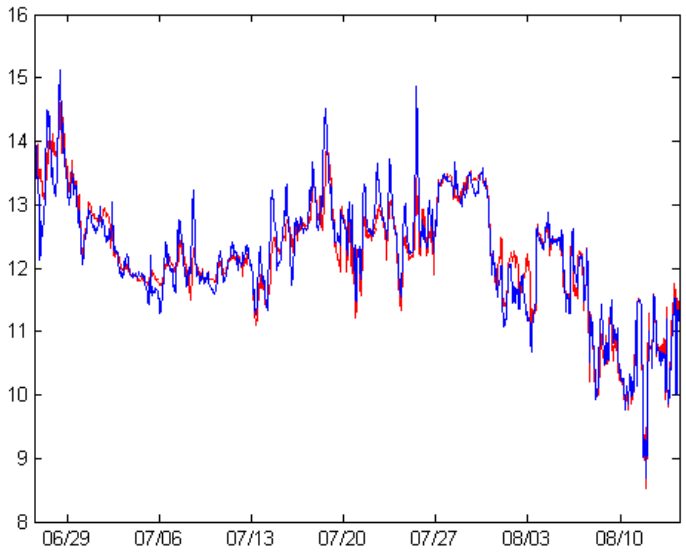

(a) Time series of the temperature measured by the NBOSI sensor and the oxygen optode AS4835. The series are full resolution data.

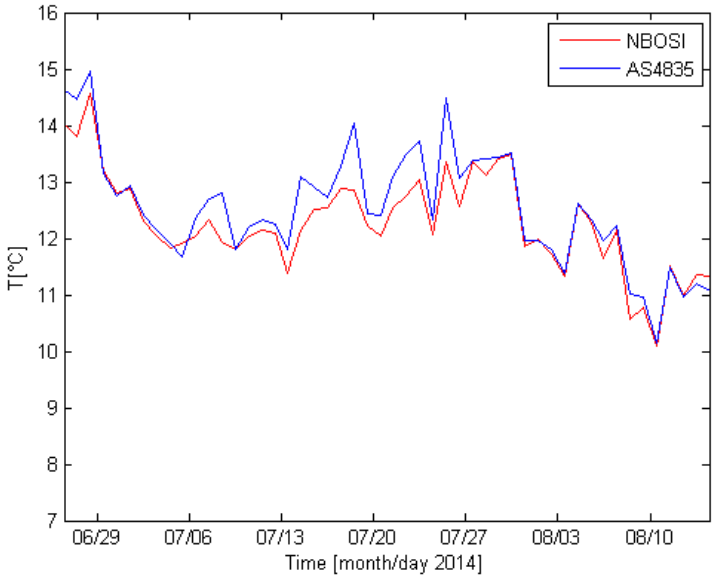

(b) Time series of the temperature measured by the NBOSI sensor and the oxygen optode AS4835. The series are daily mean.

Figure 6.7: Time series of the temperature measured by the NBOSI sensor and the oxygen optode AS4835. (a) Is full resolution data and (b) is daily mean.

6.2.1 Sea surface temperature (SST)

Figure 6.8 show a comparison of daily averaged data and a scatter plot from the SailBuoy and FOAM AMM7. The SST values compare well and have a correlation coefficient r=0.7975. FOAM AMM7 and data from the SailBuoy compare well at the beginning of the mission, clearly showing the warmer water along the coast and the drop in temperature around 10 August 2014. In the middle of the track period, around 27 July 2014, FOAM AMM7 overestimated the SST values with $\sim 1 - 2°C$, but in general the daily averaged SST collected by the SailBuoy compare well with the daily averaged SST values from FOAM AMM7.

Figure 6.9 illustrates a compared daily averaged temperature and a scatter plot from the SailBuoy and the Mercator Ocean Global Model (MGO). It has a correlation coefficient r=0.8063. MGO underestimates the SST values in the beginning, around 26 June to 06 July 2014, and in the middle of the track period, around 29 July 2014. Figure 6.9 also show the same drop in temperature around 10 August 2014, but MGO has the biggest drop on 12 August 2014.

Daily temperature values from both the models and the SailBuoy are compared in Figure 6.10. It clearly shows how both models reproduce the warm coastal water in the beginning of the campaign, even though MGO underestimates it. Both models have a decrease in temperature as the SailBuoy is leaving the coastal region and are affected by Atlantic water. Both models and the SailBuoy have an evident drop in temperature at the end of the mission. See Table 6.1 for maximum and minimum SST values for the SailBuoy, FOAM AMM7 and MGO along with the date. All three data sources have the same date for the maximum value of SST, 28 July 2014. The SailBuoy and FOAM AMM7 has the same date for the minimum value 10 August 2014, while MGO has the minimum two days later, at 12 August 2014.

Table 6.1: Maximum and minimum temperature values from the Offshore Sensing SailBuoy and the models, FOAM AMM7 and MGO.

	Max temperature		**Min temperature**	
	°C	**Date**	°C	**Date**
Offshore Sensing SailBuoy	14.6	28.06.2014	10.1	10.08.2014
FOAM AMM7	14.3	28.06.2014	10.1	10.08.2014
MGO	13.5	28.06.2014	9.8	12.08.2014

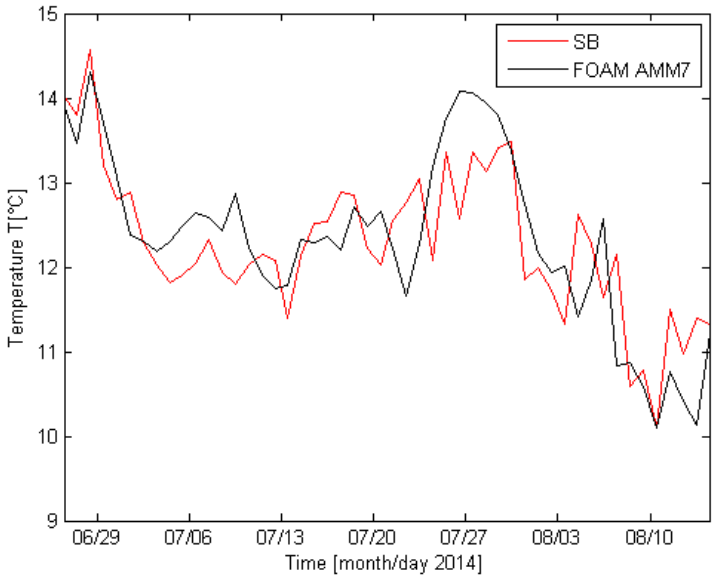

(a) Compared temperature data from the model FOAM AMM7 and the Offshore Sensing SailBuoy, daily value.

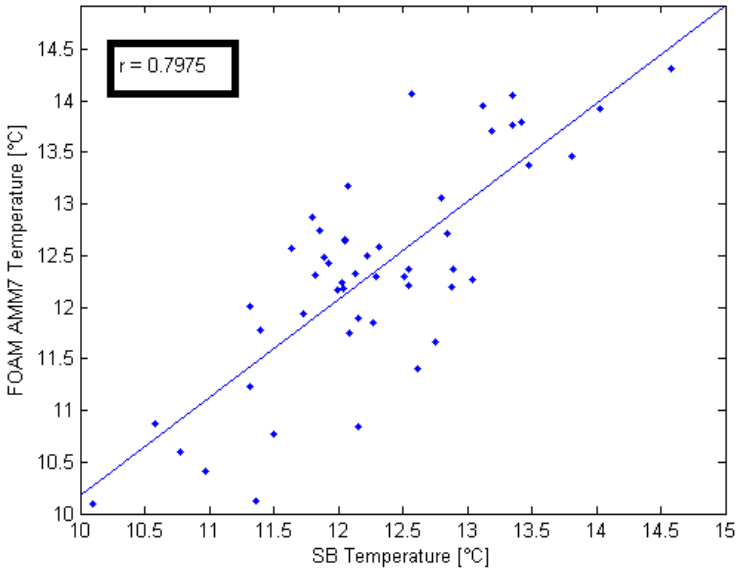

(b) Scatter plot of the temperature from the Offshore Sensing SailBuoy against the model FOAM AMM7. The correlation coefficient is r=0.7975.

Figure 6.8: Compared temperature from the Offshore Sensing SailBuoy and the model FOAM AMM7. (a) Is daily value and (b) is scatter plot of the temperature from the Offshore Sensing SailBuoy against the model FOAM AMM7.

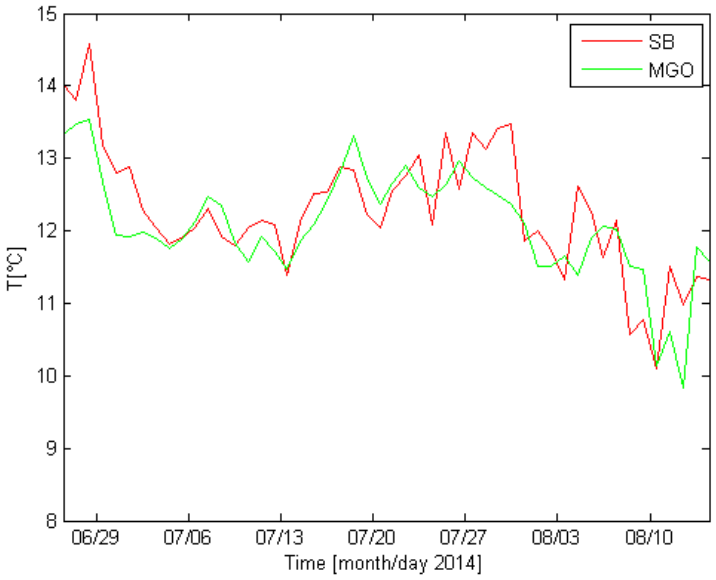

(a) Compared temperature data from the model MGO and the Offshore Sensing SailBuoy, daily value.

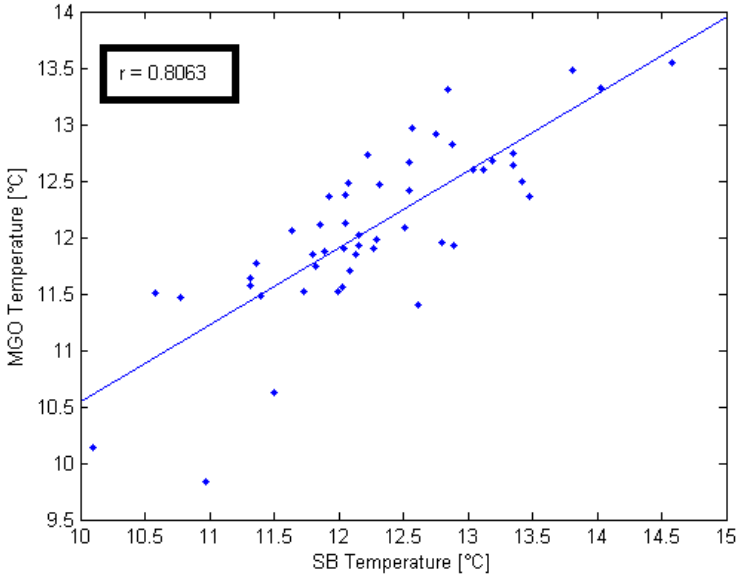

(b) Scatter plot of the temperature data from the Offshore Sensing SailBuoy against the model MGO. The correlation coefficient is r=0.8063.

Figure 6.9: Compared temperature from the Offshore Sensing SailBuoy and the model MGO. (a) Is daily value and (b) is scatter plot of the temperature from the Offshore Sensing SailBuoy against the model MGO.

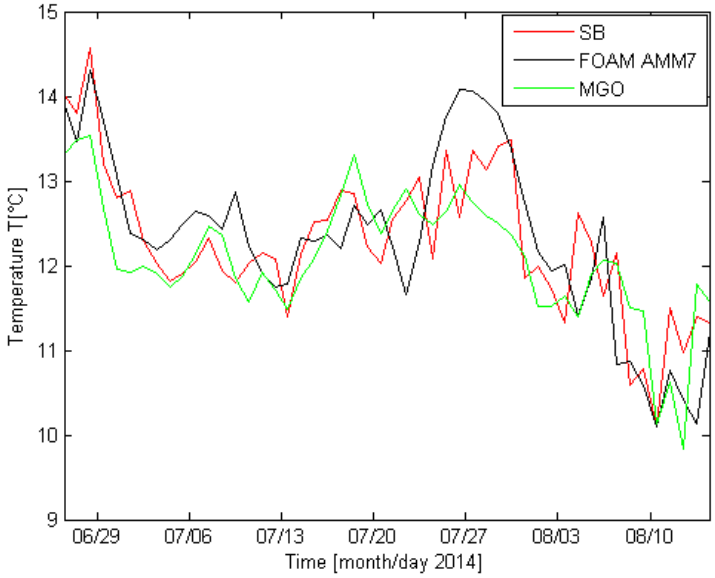

Figure 6.10: Daily average temperature data from the Offshore Sensing SailBuoy and the models FOAM AMM7 and MGO.

6.2.2 Sea surface salinity (SSS)

Daily averaged SSS measurements from the SailBuoy are compared with daily SSS output from the models FOAM AMM7 and MGO. Figure 6.11 presents the data from the SailBuoy and FOAM AMM7. The data compare well, except during the first days of tracking near the Norwegian coast, where FOAM AMM7 overestimates the SSS values with $\sim$ 1-2 psu. In total it has a correlation coefficient of r=0.9560.

In Figure 6.12 a comparison of daily averaged SSS data from the SailBuoy and SSS values from MGO is presented. The data compare well also here, except for data from the beginning of the tracking period, where MGO overestimates the SSS values with $\sim$ 1-2 psu. Totally it has a correlation coefficient of r=0.9222.

By comparing all the three SSS data sources in Figure 6.13, the models overestimate the SSS at the beginning of the campaign, near the Norwegian coast. Maximum and minimum values of SSS from the SailBuoy, FOAM AMM7 and MGO are presented in Table 6.2. The SailBuoy measured the maximum of SSS the same day as FOAM AMM7, 04 July 2014, while MGO has it maxima 6 days later, 10 July 2014. The SailBuoy, FOAM AMM7 and MGO have the minimum value of SSS on different days, 26 June 2014, 29 June 2014 and 28 June 2014 respectively.

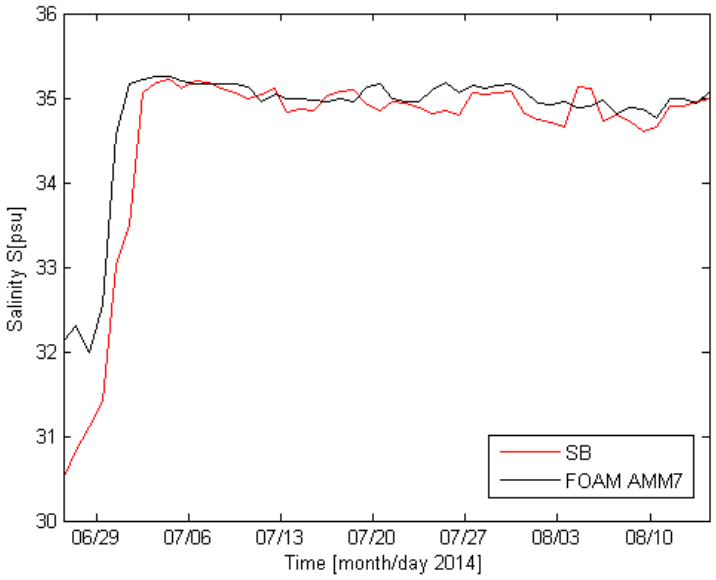

(a) Compared salinity data from the model FOAM AMM7 and the Offshore Sensing SailBuoy, daily value.

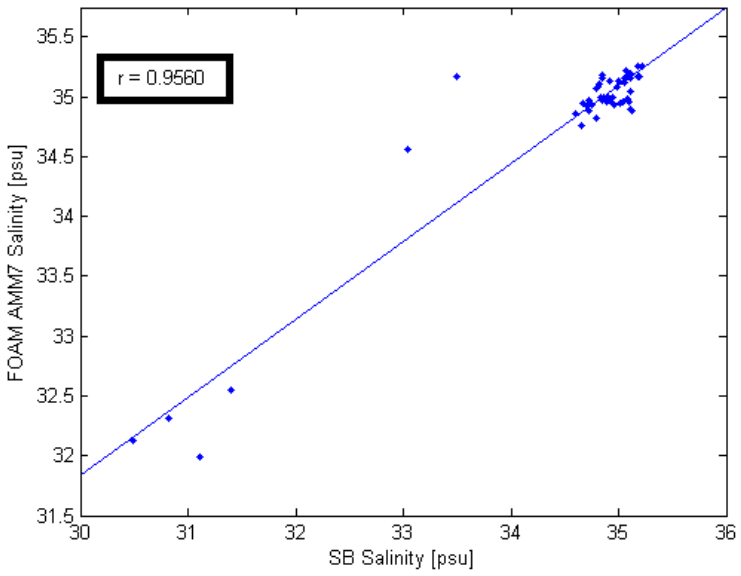

(b) Scatter plot of salinity data from the Offshore Sensing SailBuoy against the model FOAM AMM7. The correlation coefficient is r=0.9560.

Figure 6.11: Compared salinity from the Offshore Sensing SailBuoy and the model FOAM AMM7. (a) Is daily value and (b) is scatter plot of salinity data from the SailBuoy against the model FOAM AMM7.

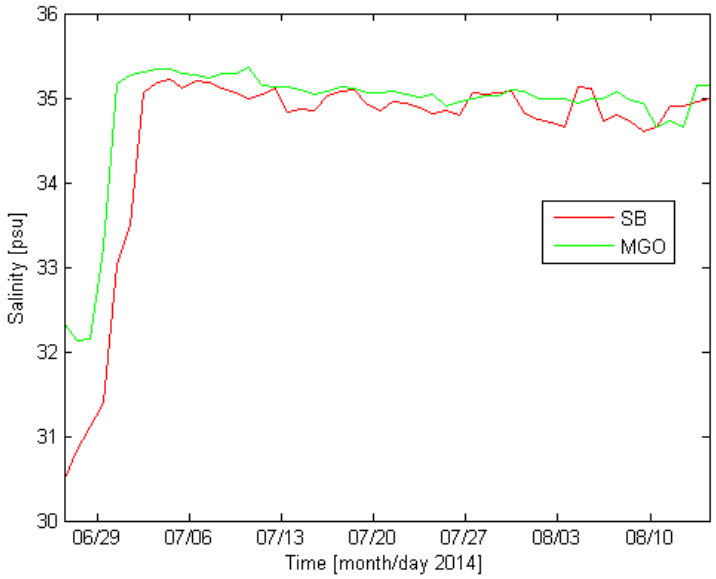

(a) Compared salinity data from the model MGO and the SailBuoy, daily value

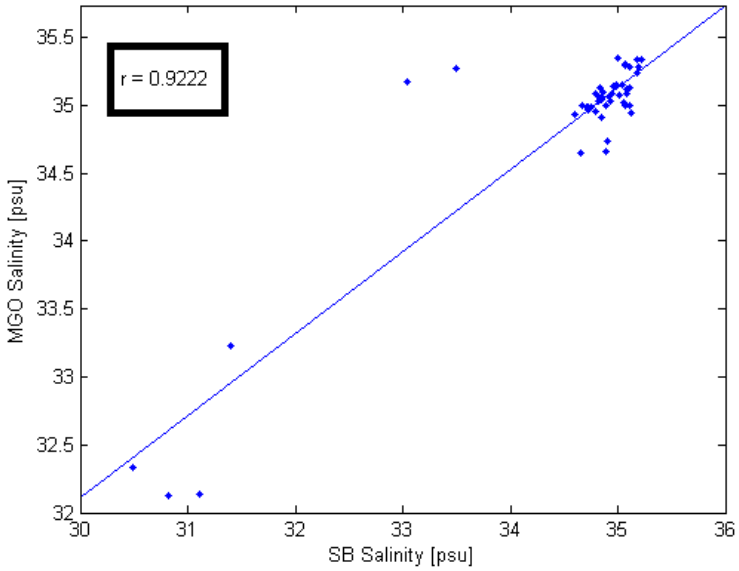

(b) Scatter plot of salinity data from the SailBuoy against the model MGO. The correlation coefficient is r=0.9222.

Figure 6.12: Compared salinity from the Offshore Sensing SailBuoy and the model MGO. (a) Is daily value and (b) is scatter plot of salinity data from the SailBuoy against the model MGO.

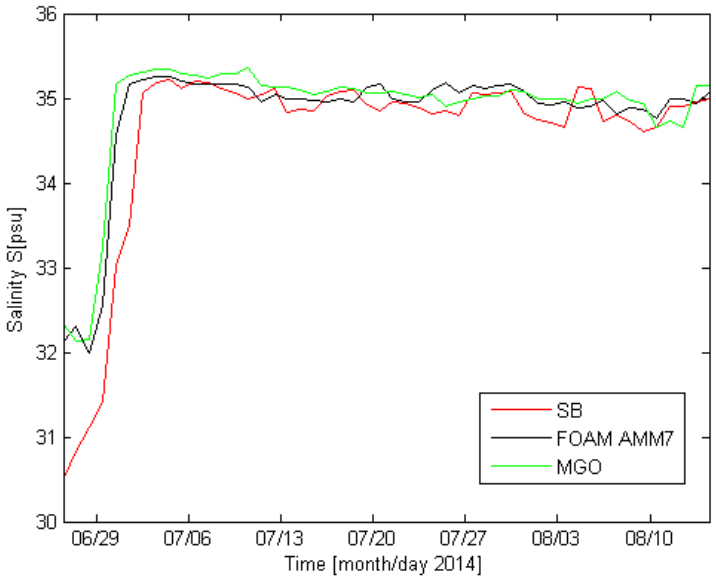

Figure 6.13: Daily average sea surface salinity data from the Offshore Sensing SailBuoy and the models FOAM AMM7 and MGO.

Table 6.2: Maximum and minimum salinity values from the Offshore Sensing SailBuoy and the models, FOAM AMM7 and MGO.

	Max salinity		**Min salinity**	
	[psu]	**Date**	**[psu]**	**Date**
SailBuoy	35.2	04.07.2014	30.5	26.06.2014
FOAM AMM7	35.3	04.07.2014	32.0	29.06.2014
MGO	35.4	10.1.2014	32.1	28.06.2014

6.3 Offshore Sensing SailBuoy data compared with remote sensing data

The daily value of SST from the SailBuoy is compared with the daily SST data from the operational sea surface temperature and sea ice analysis system, OSTIA. It shows a deviation of approximately $\sim$ 1-2$°C$. In the beginning and in the middle of the track period OSTIA underestimates the SST with $\sim$ 2-3$°C$, see Figure 6.14.

Table 6.3 presents the maximum and minimum temperature from the SailBuoy and OSTIA. The maximum values are at the same day, 28 June 2014, while the minimum value for temperature is at 11 August 2014 for OSTIA and at 10 August 2014 for the SailBuoy.

Table 6.3: Maximum and minimum sea surface temperature values from the Offshore Sensing SailBuoy and remote sensing data, OSTIA.

	Max temperature		**Min temperature**	
	[C]	**Date**	**[C]**	**Date**
SailBuoy	14.6	28.06.2014	10.1	10.08.2014
OSTIA	13.4	28.06.2014	9.6	11.08.2014

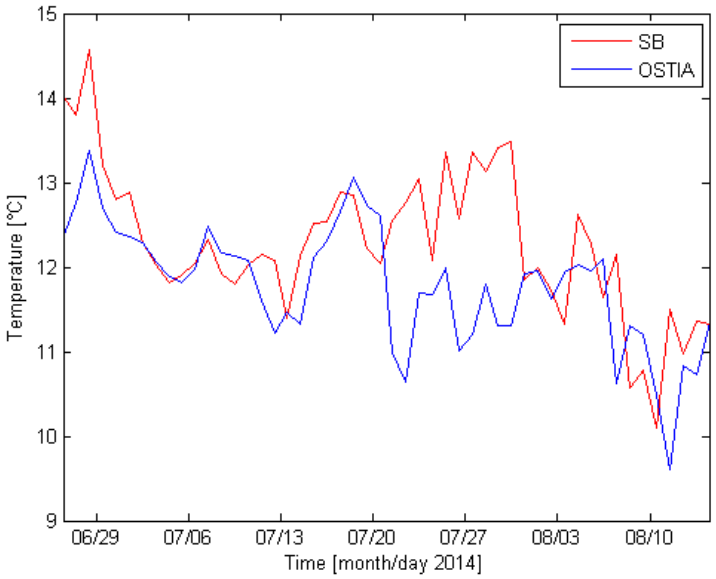

(a) Daily average temperature from the Offshore Sensing SailBuoy and remote sensing data, OSTIA.

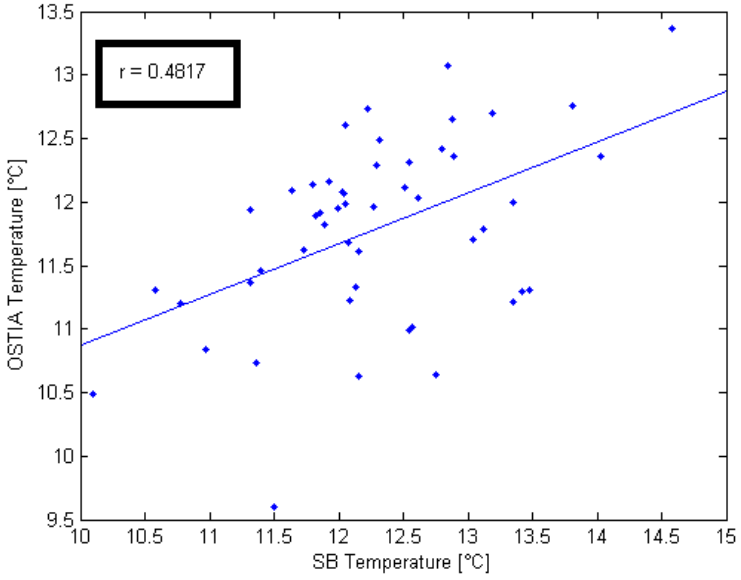

(b) Scatter plot of temperature from the Offshore Sensing SailBuoy against remote sensing data, OSTIA. The correlation coefficient is r=0.4817.

Figure 6.14: Compared temperature from the Offshore Sensing SailBuoy and remote sensing data, OSTIA. (a) Is daily value and (b) is scatter plot of temperature from the SailBuoy against the OSTIA.

Chapter 7

Discussion

There are several advantages of unmanned vehicles. Research vessels have a high daily cost for fuel and paid crew. The Offshore Sensing SailBuoy can navigate to defined way points through two-way communication by the Iridium Network (Fer and Peddie 2013). It can travel from point to point, or hold a position for longer periods. The SailBuoy uses batteries to power the on board electronics and is designed to use a small amount of power. The batteries may possibly last up to six months. For longer missions it also has the opportunity to add solar panels (Ghani et al. 2014). By comparing data from equipped sensors on the SailBuoy with ocean model simulation and remote sensing data, it can give an overview of the quality from unmanned vehicles collected data as well as validation of ocean model output and remote sensing data.

During the beginning of the track period, the SailBuoy is in a challenging area of coastal water with multiple freshwater sources and possible freshwater runoffs. Particularly SSS is a challenging parameter for coastal areas (Sætre 2007). SSS data from coastal areas are limited by satellite and expensive for research vessels. An unmanned remotely-controlled surface vehicle has the possibility to track areas with possible danger factors such as coastal areas, without any human risk.

In Figure 6.13 a comparison of SSS data from the SailBuoy and the models are illustrated. It had a good approximation, except for at the beginning of the mission. During summer and spring, March-August 2014, Norway had an averaged temperature of $2.3°C$ above normal. The amount of precipitation was normal. With an higher average temperature, more freshwater sources may occur and influence the SSS of coastal water (www.met.no/klima).

Figure 7.1a shows weekly SSS data, 26 June 2014 - 03 July 2014, from the Aquarius Instrument. The Figure is a weekly gridded map of the Northern Hemisphere downloaded from NASA Physical Oceanography Distributed Active Archive Center,

http://aquarius.umaine.edu. This is the week where the SailBuoy measured SSS near the coast. Figure 7.1b is the SSS data from the SailBuoy.

The SailBuoy SSS data were calculated from the seawater conductivity by following Fofonoff and Millard (1983). This calculation is described in Appendix A. SSS data from the SailBuoy measurements were combined with the models FOAM AMM7 and MGO output presented in Chapter 6.2.2. FOAM AMM7 had the best correlation coefficient with r = 0.9560, where r = 1 are perfectly correlated. MGO had a correlation coefficient of r = 0.9222. Both models had a positive Mean Error (ME), 0.2460 psu for FOAM AMM7 and 0.3068 psu for MGO, which may indicate overestimation of the models. It is important to remember that with ME close to zero the model does not necessary have a perfect performance for all individual days. Individual errors may cancel each other out and make the ME close to zero. Figure 6.13 presents the comparison of the models and the SailBuoy SSS data. It is also possible to see an overestimation here. The Mean Absolute Errors were 0.2857 psu for FOAM AMM7 and 0.3402 psu for MGO. Values for correlation coefficient, Mean Absolute Error and Mean Error for the SSS data are presented in Table 7.1. After all, the SSS output from the models are in alignment with the measurements from the SailBuoy, except near the coast where both models overestimate the value slightly. The lack of remote sensing data close to the coast shows that the SailBuoy is a good alternative for near coast SSS measuring.

Table 7.1: Correlation coefficient (r), Mean Absolute Error (MAE) and Mean Error (ME). The MAE and ME are [°C] for SST and [psu] for SSS.

SB	**FOAM AMM7**			**MGO**			**OSTIA**		
	r	**MAE**	**ME**	**r**	**MAE**	**ME**	**r**	**MAE**	**ME**
SST	0.7979	0.5064	+0.0619	0.8063	0.4416	-0.1847	0.4817	0.6966	-0.4990
SSS	0.9560	0.2857	+0.2462	0.9222	0.3402	+0.3068	-	-	-

The SailBuoy daily value of SST was compared with the models FOAM AMM7, MGO and remote sensing data from OSTIA. MGO had the best correlation coefficient with r = 0.8063. FOAM AMM7 was close with r = 0.7979, while OSTIA had the lowest correlation coefficient with r = 0.4817. OSTIA had the highest Mean Absolute Error of 0.6966 °C, while FOAM AMM7 and MGO had 0.5064 °C and 0.4416 °C respectively. FOAM AMM7 had a low and positive Mean Error of 0.0619 °C. Both MGO and OSTIA had a negative ME, MGO with a low bias of -0.1847 °C and OSTIA with a high bias of -0.4999 °C. Values for correlation coefficient, Mean Absolute Error and Mean Error for SST data are presented in Table 7.1. Both FOAM AMM7 and MGO had a low Mean Error. By comparing these values with Figure 6.10 which present models output with the SailBuoy SST values, a possible small overestimation of FOAM AMM7 and small underestimation of MGO are difficult to conclude on the basis of Mean Error, since Mean

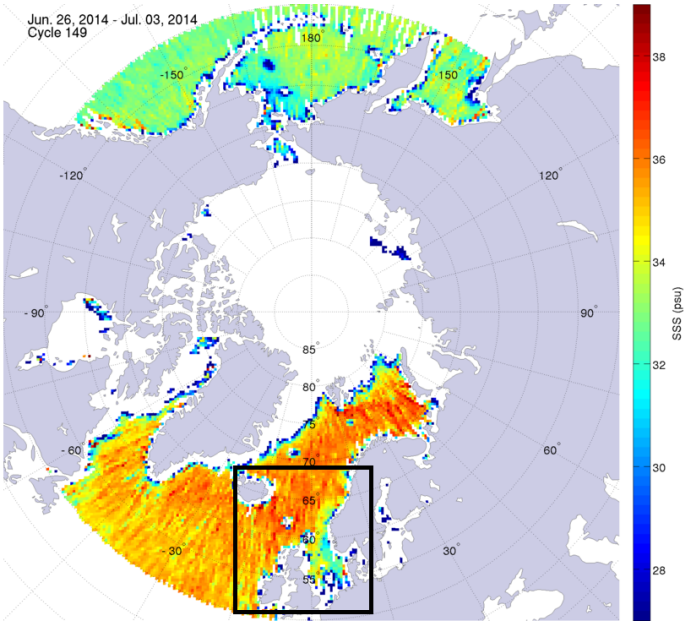

(a) Aquarius Instrument. Weekly gridded map for sea surface salinity, Northern Hemisphere, 26 June 2014 - 03. July 2014. Downloaded from http://aquarius.umaine.edu.

.

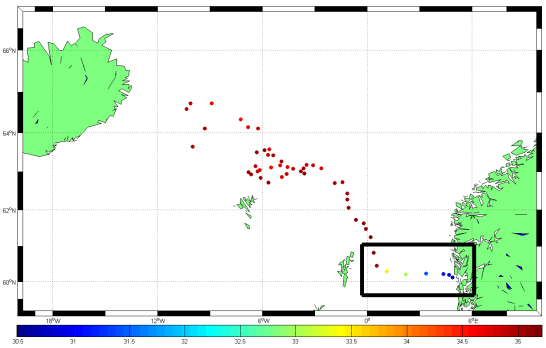

(b) Sea surface salinity from the Offshore Sensing SailBuoy. The black box indicates measurements 26 June 2014 - 03. July 2014.

Figure 7.1: Sea surface salinity near the coast compared with the Aquarius Instrument. a) Is weekly gridded map for sea surface salinity from Aquarius Instrument and b) is sea surface salinity from the Offshore Sensing SailBuoy.

Errors close to zero not necessarily mean that the models have a perfect performance for all individual days. Figure 6.14 presents SST data from the SailBuoy together with remote sense data from OSTIA and the underestimation that were expected with the negative Mean Error, is clear. The SST data from the models clearly are better aligned with the SailBuoy measurements than remote sensing data from OSTIA. This may be due to the fact that the satellite measures a large area, while the SailBuoy measures at one point and small scale features may not be picked up by the satellite.

Two days where the SST data are vary are now presented. The first period where SST data show variability is at the beginning of the mission. The SailBuoy was in coastal water outside the Norwegian coast. Figure 7.2 shows SST maps from 28 June 2014, two days after mission start and the day where all models had the highest SST. The position of the SailBuoy is shown in Figure 7.2a. The SST maps all have the same tendency, with warm Atlantic Water towards the Greenland - Scotland Ridge and a warm current along the Norwegian coast. Temperature measured by the SailBuoy was $14.6°C$. The best comparison was with FOAM AMM7 with a temperature of $14.3°C$. MGO and OSTIA have $\sim 1°C$ underestimation with $13.5°C$ and $13.4°C$ respectively.

The second period with the most varying SST output, was during the middle of the mission. SST maps for the ocean models and remote sensing together with the SailBuoy positions from 28 July 2014 are illustrated in Figure 7.3. (Note the colorbar is scaled different in Figure 7.2 and Figure 7.3) The position of the SailBuoy is presented in Figure 7.3a, north of the Faroe Islands, on the Nordic side of the Greenland - Scotland Ridge. This is an area that may be influenced by the Atlantic Water inflow as well as the possibility of polar water southward and the magnitude of the East Icelandic Current. The SailBuoy measured a temperature $13.1°C$. MGO had the nearest values with $12.6°C$, while temperature values from FOAM AMM7 were $14.0°C$ and OSTIA $11.8°C$. Still since the temperature outputs vary with $0.5 - 2.2°C$, the SST maps show some of the same characteristics. Warm coastal water along the Norwegian Coast, the Atlantic water inflow through the Iceland - Faroe Ridge and Faroe - Shetland Channel, and the cold water along Iceland with the East Icelandic Current.

Daily values of sea surface velocity from FOAM AMM7 and MGO are shown in Figure 7.4. It is a fluctuating difference in the period when the SailBuoy was northeast of the Faroe Islands, around 28-30 July can be seen. FOAM AMM7 has a strong northwest sea water velocity while MGO has a small southward velocity. Wind data from European Center for Medium Range Weather Forecast (ECMWF) reanalysis (ERA Interim), downlowded from http://apps.ecmwf.int/datasets/data/interim-full-daily/levtype=sfc/, for 28-30 July 2014 are shown in Figure 7.5. The wind data shows a light southward wind, which corresponds well with the sea surface velocity from MGO. This was the period where the SST data also were inconsistent between the SailBuoy, ocean models and remote sensing. By looking at the SST maps from FOAM AMM7 for 28 July 2014

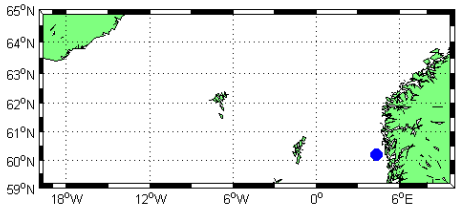

(a) Position of the Offshore Sensing SailBuoy 28 June 2014

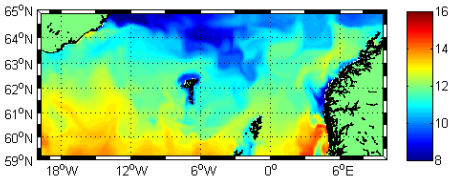

(b) SST 28 June 2014 from the model FOAM AMM7.

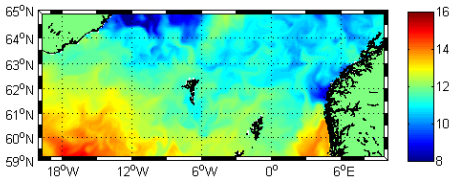

(c) SST 28 June 2014 from the model MGO

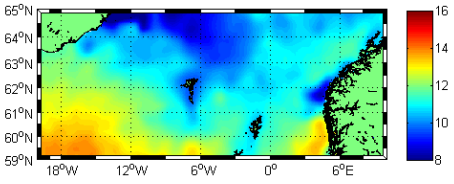

(d) SST 28 June 2014 from remote sensing data, OSTIA.

Figure 7.2: Position of the Offshore Sensing SailBuoy and SST data from the models FOAM AMM7 and MGO, and remote sensing data from OSTIA on 28 June 2014.

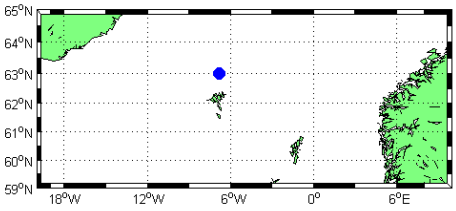

(a) Position of the Offshore Sensing SailBuoy 28 July 2014

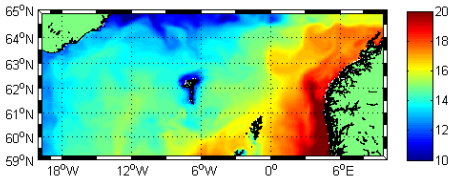

(b) SST 28 July 2014 from the model FOAM AMM7.

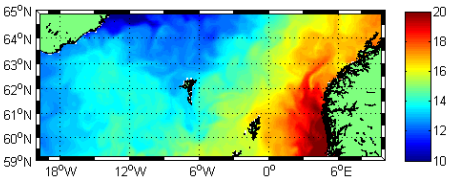

(c) SST 28 July 2014 from the model MGO

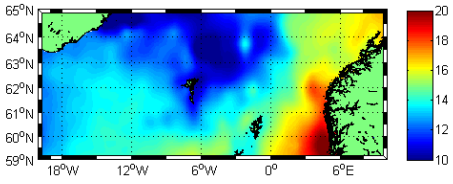

(d) SST 28 July 2014 from remote sensing data, OSTIA.

Figure 7.3: Position of the Offshore Sensing SailBuoy and SST data from the models FOAM AMM7 and MGO, and remote sensing data from OSTIA on 28 July 2014.

in Figure 7.3b, FOAM AMM7 has a clear stronger inflow of Atlantic Water then MGO and OSTIA. This corresponds well with the strong northward velocity, and may be the reason for the overestimation of SST in this period. This illustrates the possibility to equip the SailBuoy with meteorological sensors to verify meteorological parameters as well.

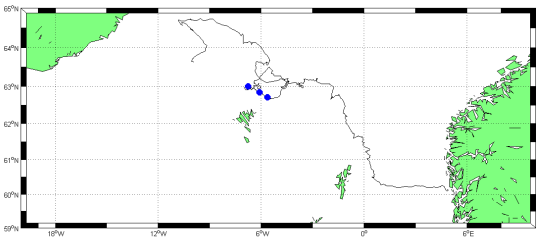

(a) The track of the Offshore Sensing SailBuoy together with the positions where the models FOAM AMM7 and MGO had a big difference in sea water velocity.

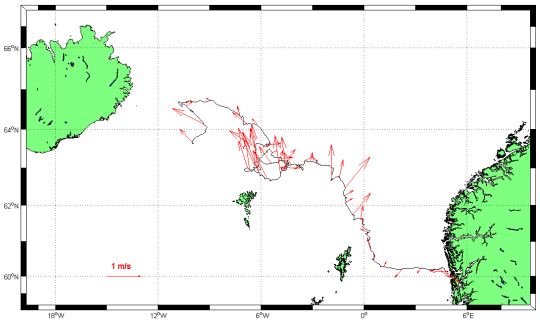

(b) Sea water velocity $[ms^{-1}]$ from the model FOAM AMM7.

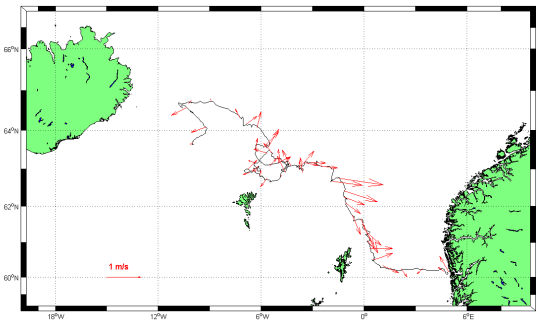

(c) Sea water velocity $[ms^{-1}]$ from the model MGO.

Figure 7.4: Track of the Offshore Sensing SailBuoy with sea water velocity vectors from the models (b) FOAM AMM7 and (c) MGO, $[ms^{-1}]$.

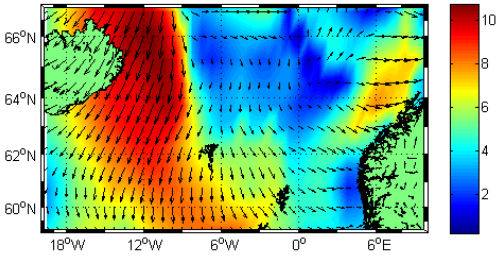

(a) Wind data from European Center for Medium Range Weather Forecast (ECMWF) reanalysis (ERA Interim) for 28 July 2014.

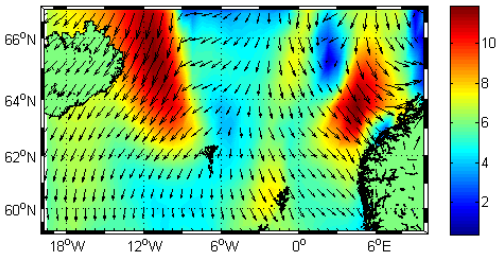

(b) Wind data from European Center for Medium Range Weather Forecast (ECMWF) reanalysis (ERA Interim) for 29 July 2014.

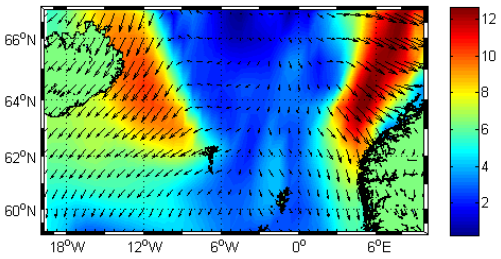

(c) Wind data from ECMWF 30 July 2014.

Figure 7.5: Wind data from European Center for Medium Range Weather Forecast (ECMWF) reanalysis (ERA Interim) for 28 - 30 July 2014. The colour indicates the wind speed $[ms^{-1}]$, and the arrows are the direction.

Chapter 8

Summary

The main aim of this thesis was to investigate and increase the understanding of usefulness of an unmanned surface vehicle and validate ocean model simulations and remote sensing data. The Offshore Sensing SailBuoy is a 100% wind driven unmanned remotely-controlled surface vehicle, capable of traveling up to 6 months. The possibilities diversity and varying sensors make the application area large. In this thesis, a mission in the North Atlantic has been investigated. In situ ocean surface data of temperature, conductivity and dissolved oxygen have been collected, together with the position of the vehicle. The velocity is deduced from its displacement between known longitude-latitude positions and known time steps.

The tracking period was affected by a front between water masses with different characteristics. Along the Norwegian coast, coastal water with salinity under 35 psu influenced by freshwater run-off from Norway was found. This region shows variation both in ocean model output and remote sensing data with regard to sea surface temperature and calculated sea surface salinity from the conductivity measured by the SailBuoy. Sea surface salinity measured in coastal areas are still limited by remote sensing and this shows that the SailBuoy is a good alternative for near coast sea surface salinity measuring.

When the SailBuoy left the coastal area, inflow of Atlantic water from the North Atlantic Current was detected. The salinity stabilized around 35 psu and correlated well to the ocean model output.

Overall, validation of the measured near surface properties from the SailBuoy with ocean models and remote sensing, the in-situ ocean surface data from the SailBuoy is of high quality. The SailBuoy is clearly useful to validate model and remote sensing data. In this thesis, the positions from the ocean models and remote sensing are chosen by finding the nearest grid point to the average daily position of the SailBuoy. For further studies an average over adjacent grid cells could be considered instead of single grid points. It

would improve the knowledge of how the number of grid cells may change the validation results and account for the daily movement of the SailBuoy.

Currently, the SailBuoy has been on a mission in the North Sea to measure waves as a stationary buoy. It has been a successful campaign. Together with the comparison of sea surface velocity from ocean models and wind data from European Center for Medium Range Weather Forecast (ECMWF) reanalysis (ERA Interim), it illustrates the magnitude of possibilities for equipped sensors on the SailBuoy.

The SailBuoy is a low cost and time saving alternative when combining it with bigger research vessels. An unmanned remotely-controlled surface vehicle also enhances the possibility to track areas with possible danger factors such as coastal areas, without any human risk.

Appendix A

Calculation of salinity

The salinity of seawater is defined by its electoral conductivity and calculated by following Fofonoff and Millard (1983).

The conductivity ratio is defined

$$R = \frac{C(S,t,p)}{C(35,15,0)} \tag{A.1}$$

where C(35,15,0) is the conductivity of standard KCl solution being $32.4356 gkg^{-1}$, salinity $35psu$, temperature $15°C$ and atmospheric pressure.

The conductivity factor may be factories into three parts;

$$R = R_p * R_t * r_t \tag{A.2}$$

where

$$R_p(S,t,p) = \frac{C(S,t,p)}{C(S,t,0)} \tag{A.3}$$

$$R_t(S,t) = \frac{C(S,t,0)}{C(35,t,0)} \tag{A.4}$$

$$r_t(t) = \frac{C(35,t,0)}{C(35,15,0)} \tag{A.5}$$

The ratio r_t is given by:

$$r_t = c_0 + c_1 t + c_2 t^2 + c_3 t^3 + c_4 t^4 \tag{A.6}$$

where

$c_0 = 0.6766097$

$c_1 = 2.00564$

$c_2 = 1.104259$

$c_3 = -6.9698$

$c_4 = 1.0031$

The ratio R_p is given by:

$$R_p = 1 + \frac{p(e_1 + e_2 p + e_3 p^2)}{1 + d_1 t + d_2 t^2 + (d_3 + d_4 t)R} \tag{A.7}$$

where

$e_1 = 2.070$

$e_2 = -6.370$

$e_3 = 3.989$

$d_1 = 3.426$

$d_2 = 4.464$

$d_3 = 4.215$

$d_4 = -3.107$

The ratio R_t is given by:

$$R_t = \frac{R}{R_p * r_t} \tag{A.8}$$

The salinity is defined by the following equation:

$$S = a_0 + a_1 R^{1/2} + a_2 R_t + a_3 R_t^{3/2} + a_4 R_t^2 + a_5 R_t^{5/2} + \Delta S \tag{A.9}$$

$$\Delta S = \frac{(t-15)}{1 + k(t-15)} b_0 + b_1 R^{1/2} + b_2 R_t + b_3 R_t^{3/2} + b_4 R_t^2 + b_5 R_t^{5/2} \tag{A.10}$$

where

$a_0 = 0.0080$

$a_1 = -0.1692$

$a_2 = 25.3851$

$a_3 = 14.0941$

$a_4 = -7.0261$

$a_5 = 2.7081$

$b_0 = 0.0005$

$b_1 = -0.0056$

$b_2 = -0.0066$

$b_3 = -0.0375$

$b_4 = 0.0636$

$b_5 = -0.0144$

$k = 0.0162$

Appendix B

Daily values and positions

Figures B.1, B.2 and B.3 present a comparison of grid points and positions from the ocean models, The Forecast Ocean Assimilation Model 7 km Atlantic Margin Model(FOAM AMM7) and The Operational Mercator global Ocean analysis and forecast system (MGO), remote sensing, Global Ocean Sea surface temperature and Sea Ice analysis (OSTIA), and the Offshore Sensing SailBuoy. In this thesis, the positions from ocean models and remote sensing are chosen by finding the nearest grid point to the average daily position of the SailBuoy.

A table of positions and daily values of SST, SSS are presented for the SailBuoy in Table B.1 and B.2, for FOAM AMM7 in Table B.3 and B.4, for MGO in Table B.5 and B.6 and for OSTIA in Table B.7 and B.8.

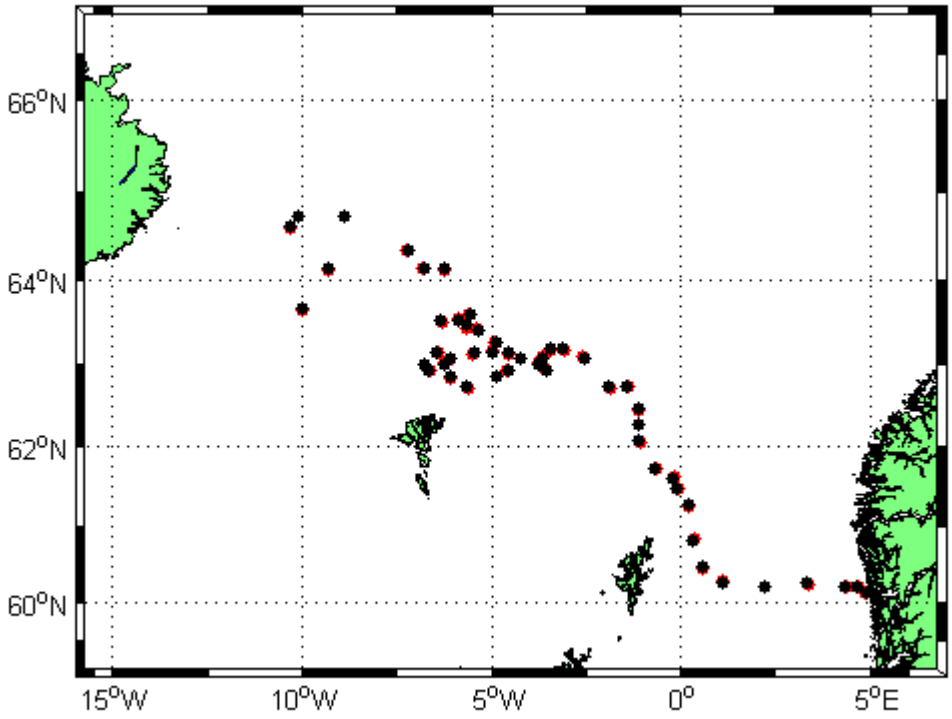

Figure B.1: Daily positions for the SailBuoy (red) compared with grid points for the FOAM AMM7 (black).

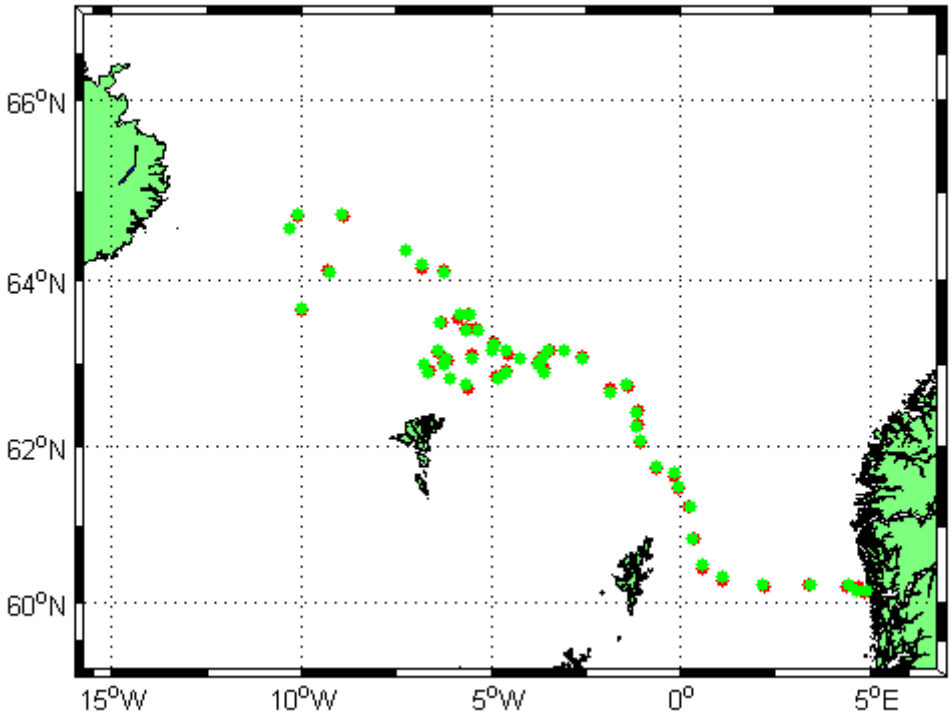

Figure B.2: Daily positions for the SailBuoy (red) compared with grid points for the MGO (green).

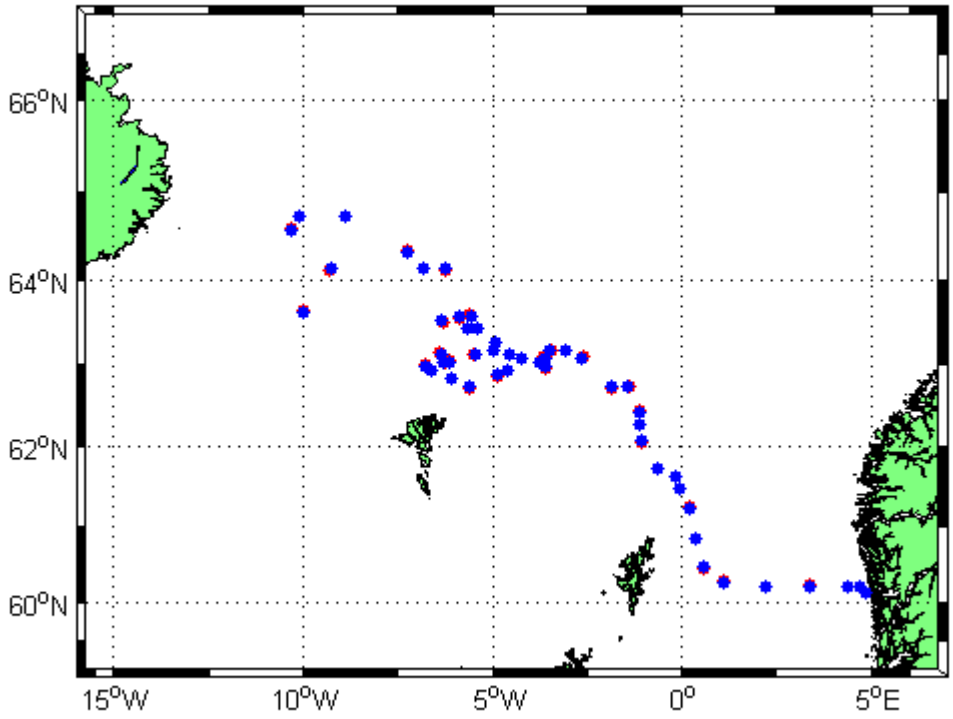

Figure B.3: Daily positions for the SailBuoy (red) compared with daily grid points for the OSTIA (blue).

Table B.1: Position (lon/lat), sea surface temperature [°C] and sea surface salinity [psu] interpolated daily value from the Offshore Sensing SailBuoy 26.06.2014 - 31.07.2014.

DATE	**SailBuoy**			
	LON	**LAT**	**SST**	**SSS**
26.06.2014	4,88055799995396	60,1255940000317	14,0	30,5
27.06.2014	4,69533800001431	60,2001239999826	13,8	30,8
28.06.2014	4,37899300004597	60,2206760000123	14,6	31,1
29.06.2014	3,38623600008451	60,2391060000038	13,2	31,4
30.06.2014	2,20493900009545	60,2142630000067	12,8	33,0
01.07.2014	1,11787000003928	60,2936969999965	12,9	33,5
02.07.2014	0,562759000110311	60,4581339999590	12,3	35,1
03.07.2014	0,375114000031214	60,8240559999348	12,0	35,2
04.07.2014	0,211061999899350	61,2476609999959	11,8	35,2
05.07.2014	-0,0622429999674056	61,4775749999857	11,9	35,1
06.07.2014	-0,181604999906039	61,6269159999890	12,1	35,2
07.07.2014	-0,625794999948507	61,7289099999883	12,3	35,2
08.07.2014	-1,06948400003652	62,0522159999815	11,9	35,1
09.07.2014	-1,13150549998970	62,2705064999920	11,8	35,1
10.07.2014	-1,12757300003846	62,4370229999644	12,0	35,0
11.07.2014	-1,40591199998932	62,7255549999635	12,2	35,0
12.07.2014	-1,84956149994459	62,7022705000284	12,1	35,1
13.07.2014	-2,60813149987812	63,0938864999724	11,4	34,8
14.07.2014	-3,09683699996372	63,1716764999953	12,1	34,9
15.07.2014	-3,46301750000300	63,1795094999923	12,5	34,8
16.07.2014	-3,63404899996393	63,0873249999962	12,5	35,0
17.07.2014	-3,77678500000272	63,0161675000128	12,9	35,1
18.07.2014	-3,58247099997287	62,9574225000123	12,8	35,1
19.07.2014	-4,23889549991343	63,0807625000166	12,2	34,9
20.07.2014	-4,61097150009823	62,9407179999900	12,0	34,8
21.07.2014	-4,90588849994318	63,2752080000020	12,6	35,0
22.07.2014	-5,37392849994753	63,4224374999812	12,8	34,9
23.07.2014	-5,67507350000038	63,4404275000128	13,0	34,9
24.07.2014	-6,39505299999161	63,1466855000148	12,1	34,8
25.07.2014	-6,26498650003558	63,0154160000126	13,4	34,9
26.07.2014	-6,14133749996486	63,0466264999713	12,6	34,8
27.07.2014	-6,63676699994955	62,9287029999981	13,4	35,1
28.07.2014	-6,77521750008363	62,9954950000027	13,1	35,0
29.07.2014	-6,08392050000768	62,8427220000340	13,4	35,1
30.07.2014	-5,63482700001773	62,7143740000355	13,5	35,1
31.07.2014	-4,86700100002983	62,8637609999513	11,9	34,8

Table B.2: Position (lon/lat), sea surface temperature [°C] and sea surface salinity [psu] interpolated daily value from the Offshore Sensing SailBuoy 01.08.2014 - 14.08.2014.

DATE	**SailBuoy**			
	LON	**LAT**	**SST**	**SSS**
01.08.2014	-4,55796849991267	63,1259019999828	12,0	34,7
02.08.2014	-4,96374699995297	63,1677910000097	11,7	34,7
03.08.2014	-5,49319149993261	63,1169890000086	11,3	34,7
04.08.2014	-6,30741699999119	63,5035929999632	12,6	35,1
05.08.2014	-5,86249699999543	63,5557080000019	12,3	35,1
06.08.2014	-5,58797900002219	63,5841529999738	11,6	34,7
07.08.2014	-6,23230999988427	64,1027029999578	12,1	34,8
08.08.2014	-6,80832999996603	64,1347960000081	10,6	34,7
09.08.2014	-7,22845999990976	64,3361839999537	10,8	34,6
10.08.2014	-8,88097949988771	64,7310829999927	10,1	34,7
11.08.2014	-10,1145914999479	64,7227134999960	11,5	34,9
12.08.2014	-10,3349265001227	64,5877660000410	11,0	34,9
13.08.2014	-9,29240800009785	64,1051405000393	11,4	35,0
14.08.2014	-9,98095700003684	63,6446730000003	11,3	35,0

Table B.3: Model grid-point (lon/lat), sea surface temperature [°C] and sea surface salinity [psu] daily value output from the ocean model FOAM AMM7 26.06.2014 - 31.07.2014.

DATE	**FOAM AMM7**			
	LON	**LAT**	**SST**	**SSS**
26.06.2014	4,8886399	60,134338	13,9	32,1
27.06.2014	4,6664200	60,201012	13,5	32,3
28.06.2014	4,3330898	60,201012	14,3	32,0
29.06.2014	3,3331001	60,267681	13,7	32,6
30.06.2014	2,2219999	60,201012	13,1	34,6
01.07.2014	1,1109000	60,267681	12,4	35,2
02.07.2014	0,55535001	60,467690	12,3	35,2
03.07.2014	0,33313000	60,801041	12,2	35,3
04.07.2014	0,22202000	61,267731	12,3	35,3
05.07.2014	-0,11131000	61,467739	12,5	35,2
06.07.2014	-0,22242001	61,601082	12,6	35,2
07.07.2014	-0,66685998	61,734421	12,6	35,2
08.07.2014	-1,1113000	62,067768	12,4	35,2
09.07.2014	-1,1113000	62,267780	12,9	35,2
10.07.2014	-1,1113000	62,467789	12,2	35,1
11.07.2014	-1,4446300	62,734470	11,9	34,9
12.07.2014	-1,8890700	62,734470	11,7	35,1
13.07.2014	-2,5557301	63,067822	11,8	35,0
14.07.2014	-3,1112800	63,201160	12,3	35,0
15.07.2014	-3,4446101	63,201160	12,3	34,9
16.07.2014	-3,6668301	63,067822	12,4	34,9
17.07.2014	-3,7779400	63,001148	12,2	35,0
18.07.2014	-3,5557201	62,934479	12,7	34,9
19.07.2014	-4,2223802	63,067822	12,5	35,1
20.07.2014	-4,5557098	62,934479	12,7	35,2
21.07.2014	-4,8890400	63,267830	12,2	35,0
22.07.2014	-5,3334799	63,401169	11,7	35,0
23.07.2014	-5,6668100	63,467838	12,3	35,0
24.07.2014	-6,4445801	63,134491	13,2	35,1
25.07.2014	-6,2223601	63,001148	13,8	35,2
26.07.2014	-6,1112499	63,067822	14,1	35,1
27.07.2014	-6,6668000	62,934479	14,1	35,2
28.07.2014	-6,7779102	63,001148	13,9	35,1
29.07.2014	-6,1112499	62,867809	13,8	35,2
30.07.2014	-5,6668100	62,734470	13,4	35,2
31.07.2014	-4,8890400	62,867809	12,7	35,1

Table B.4: Model grid-point (lon/lat), sea surface temperature [°C] and sea surface salinity [psu] daily value output from the ocean model FOAM AMM7 01.08.2014 - 14.08.2014.

DATE	**FOAM AMM7**			
	LON	**LAT**	**SST**	**SSS**
01.08.2014	-4,5557098	63,134491	12,2	34,9
02.08.2014	-5,0001502	63,134491	11,9	34,9
03.08.2014	-5,4445901	63,134491	12,0	34,9
04.08.2014	-6,3334699	63,534512	11,4	34,9
05.08.2014	-5,8890300	63,534512	11,9	34,9
06.08.2014	-5,5556998	63,601181	12,6	35,0
07.08.2014	-6,2223601	64,134537	10,8	34,8
08.08.2014	-6,7779102	64,134537	10,9	34,9
09.08.2014	-7,2223501	64,334549	10,6	34,9
10.08.2014	-8,8889999	64,734573	10,1	34,8
11.08.2014	-10,111210	64,734573	10,8	35,0
12.08.2014	-10,333430	64,601227	10,4	35,0
13.08.2014	-9,3334398	64,134537	10,1	34,9
14.08.2014	-10,000100	63,667850	11,2	35,1

Table B.5: Model grid-point (lon/lat), sea surface temperature [°C] and sea surface salinity [psu] daily value output from the ocean model MGO 26.06.2014 - 31.07.2014.

DATE	**MGO**			
	LON	**LAT**	**SST**	**SSS**
26.06.2014	4,9166718	60,166672	13,3	32,3
27.06.2014	4,6666718	60,166672	13,5	32,1
28.06.2014	4,4166718	60,250000	13,5	32,1
29.06.2014	3,4166718	60,250000	12,7	33,2
30.06.2014	2,1666718	60,250000	11,9	35,2
01.07.2014	1,0833435	60,333344	11,9	35,3
02.07.2014	0,58334351	60,500000	12,0	35,3
03.07.2014	0,33334351	60,833344	11,9	35,3
04.07.2014	0,25000000	61,250000	11,7	35,3
05.07.2014	-0,083328247	61,500000	11,9	35,3
06.07.2014	-0,16665649	61,666672	12,1	35,3
07.07.2014	-0,66665649	61,750000	12,5	35,2
08.07.2014	-1,0833282	62,083344	12,4	35,3
09.07.2014	-1,1666565	62,250000	11,8	35,3
10.07.2014	-1,1666565	62,416672	11,6	35,4
11.07.2014	-1,4166565	62,750000	11,9	35,2
12.07.2014	-1,8333282	62,666672	11,7	35,1
13.07.2014	-2,5833282	63,083344	11,5	35,1
14.07.2014	-3,0833282	63,166672	11,9	35,1
15.07.2014	-3,5000000	63,166672	12,1	35,0
16.07.2014	-3,6666565	63,083344	12,4	35,1
17.07.2014	-3,7500000	63,000000	12,8	35,1
18.07.2014	-3,5833282	62,916672	13,3	35,1
19.07.2014	-4,2500000	63,083344	12,7	35,1
20.07.2014	-4,5833282	62,916672	12,4	35,1
21.07.2014	-4,9166565	63,250000	12,7	35,1
22.07.2014	-5,3333282	63,416672	12,9	35,0
23.07.2014	-5,6666565	63,416672	12,6	35,0
24.07.2014	-6,4166565	63,416672	12,5	35,0
25.07.2014	-6,2500000	63,000000	12,6	34,9
26.07.2014	-6,1666565	63,083344	13,0	34,9
27.07.2014	-6,6666565	62,916672	12,7	35,0
28.07.2014	-6,7500000	63,000000	12,6	35,0
29.07.2014	-6,0833282	62,833344	12,5	35,0
30.07.2014	-5,6666565	62,750000	12,4	35,1
31.07.2014	-4,8333282	62,833344	12,1	35,1

Table B.6: Model grid-point (lon/lat), sea surface temperature [°C] and sea surface salinity [psu] daily value output from the ocean model MGO 01.08.2014 - 14.08.2014.

DATE	**MGO**			
	LON	**LAT**	**SST**	**SSS**
01.08.2014	-4,5833282	63,166672	11,5	35,0
02.08.2014	-5,0000000	63,166672	11,5	35,0
03.08.2014	-5,5000000	63,083344	11,6	35,0
04.08.2014	-6,3333282	63,500000	11,4	34,9
05.08.2014	-5,8333282	63,583344	11,9	35,0
06.08.2014	-5,5833282	63,583344	12,1	35,0
07.08.2014	-6,2500000	64,083344	12,0	35,1
08.08.2014	-6,8333282	64,166672	11,5	35,0
09.08.2014	-7,2500000	64,333344	11,5	34,9
10.08.2014	-8,9166565	64,750000	10,1	34,7
11.08.2014	-10,083328	64,750000	10,6	34,7
12.08.2014	-10,333328	64,583344	9,8	34,7
13.08.2014	-9,2500000	64,083344	11,8	35,1
14.08.2014	-10,0000000	63,666672	11,6	35,1

Table B.7: Position (lon/lat), sea surface temperature [°C] daily value output from the remote sensing data OSTIA 26.06.2014 - 31.07.2014.

DATE	**OSTIA**		
	LON	**LAT**	**SST**
26.06.2014	4,8750000	60,125000	12,4
27.06.2014	4,6750002	60,224998	12,8
28.06.2014	4,3750000	60,224998	13,4
29.06.2014	3,3750000	60,224998	12,7
30.06.2014	2,2249999	60,224998	12,4
01.07.2014	1,1250000	60,275002	12,4
02.07.2014	0,57499999	60,474998	12,3
03.07.2014	0,37500000	60,825001	12,1
04.07.2014	0,22499999	61,224998	11,9
05.07.2014	-0,075000003	61,474998	11,8
06.07.2014	-0,17500000	61,625000	12,0
07.07.2014	-0,62500000	61,724998	12,5
08.07.2014	-1,0750000	62,075001	12,2
09.07.2014	-1,1250000	62,275002	12,1
10.07.2014	-1,1250000	62,424999	12,1
11.07.2014	-1,4250000	62,724998	11,6
12.07.2014	-1,8750000	62,724998	11,2
13.07.2014	-2,6250000	63,075001	11,5
14.07.2014	-3,0750000	63,174999	11,3
15.07.2014	-3,4749999	63,174999	12,1
16.07.2014	-3,6250000	63,075001	12,3
17.07.2014	-3,7750001	63,025002	12,6
18.07.2014	-3,5750000	62,974998	13,1
19.07.2014	-4,2249999	63,075001	12,7
20.07.2014	-4,6250000	62,924999	12,6
21.07.2014	-4,9250002	63,275002	11,0
22.07.2014	-5,3750000	63,424999	10,6
23.07.2014	-5,6750002	63,424999	11,7
24.07.2014	-6,3750000	63,125000	11,8
25.07.2014	-6,2750001	63,025002	12,0
26.07.2014	-6,1250000	63,025002	11,0
27.07.2014	-6,6250000	62,924999	11,2
28.07.2014	-6,7750001	62,974998	11,8
29.07.2014	-6,0749998	62,825001	11,3
30.07.2014	-5,6250000	62,724998	11,3
31.07.2014	-4,8750000	62,875000	11,9

Table B.8: Position (lon/lat), sea surface temperature [°C] daily value output from the remote sensing data OSTIA 01.08.2014 - 14.08.2014.

DATE	**OSTIA**		
	LON	**LAT**	**SST**
01.08.2014	-4,5749998	63,125000	11,9
02.08.2014	-4,9749999	63,174999	11,6
03.08.2014	-5,4749999	63,125000	11,9
04.08.2014	-6,3249998	63,525002	12,0
05.08.2014	-5,8750000	63,575001	12,0
06.08.2014	-5,5749998	63,575001	12,1
07.08.2014	-6,2249999	64,125000	10,6
08.08.2014	-6,8249998	64,125000	11,3
09.08.2014	-7,2249999	64,324997	11,2
10.08.2014	-8,8750000	64,724998	10,5
11.08.2014	-10,125000	64,724998	9,6
12.08.2014	-10,325000	64,574997	10,8
13.08.2014	-9,2749996	64,125000	10,7
14.08.2014	-9,9750004	63,625000	11,4

References

Aanderaa. Oxygen optode 4835, http://www.aanderaa.com/media/pdfs/oxygen-optode-4835.pdf.

Arakawa, A. and V. R. Lamb (1981). A potential enstrophy and energy conserving scheme for the shallow water equations. *Monthly Weather Review 109*(1), 18–36.

Blockley, E., M. Martin, A. McLaren, A. Ryan, J. Waters, D. Lea, I. Mirouze, K. Peterson, A. Sellar, and D. Storkey (2013). Recent development of the met office operational ocean forecasting system: an overview and assessment of the new global foam forecasts. *Geoscientific Model Development Discussions 6*, 6219–6278.

Bloom, S., L. Takacs, A. Da Silva, and D. Ledvina (1996). Data assimilation using incremental analysis updates. *Monthly Weather Review 124*(6), 1256–1271.

Brown, E., A. Colling, D. Park, J. Phillips, D. Rothery, and J. Wright (1995). *Seawater: its composition, properties and behaviour*. Butterworth-Heinemann.

Caccia, M., M. Bibuli, R. Bono, and G. Bruzzone (2008). Basic navigation, guidance and control of an unmanned surface vehicle. *Autonomous Robots 25*(4), 349–365.

Caccia, M., R. Bono, G. Bruzzone, E. Spirandelli, G. Veruggio, A. Stortini, and G. Capodaglio (2005). Sampling sea surfaces with sesamo: an autonomous craft for the study of sea-air interactions. *Robotics & Automation Magazine, IEEE 12*(3), 95–105.

Donlon, C. J., M. Martin, J. Stark, J. Roberts-Jones, E. Fiedler, and W. Wimmer (2012). The operational sea surface temperature and sea ice analysis (ostia) system. *Remote Sensing of Environment 116*, 140–158.

Fer, I. and D. Peddie (2012). Navigation performance of the sailbuoy. *Bergen, Scotland mission 12*.

Fer, I. and D. Peddie (2013). Near surface oceanographic measurements using the sailbuoy. pp. 1–15.

Fofonoff, N. P. and R. C. Millard (1983). Algorithms for computation of fundamental properties of seawater.

Ghani, M. H., L. R. Hole, I. Fer, V. H. Kourafalou, N. Wienders, H. Kang, K. Drushka, and D. Peddie (2014). The sailbuoy remotely-controlled unmanned vessel: Measurements of near surface temperature, salinity and oxygen concentration in the northern gulf of mexico. *Methods in Oceanography 10*, 104–121.

Gytre, T. (2004). 7.13 havets oppløste oksygen-hvor kommer det fra, hvorfor er det så nødvendig og hvordan måler vi det?

Hansen, B. and S. Østerhus (2000). North atlantic–nordic seas exchanges. *Progress in Oceanography 45*(2), 109–208.

Helland-Hansen, B. and F. Nansen (1909). The norwegian sea. *Report on Norwegian fishery and marine investigations 2*(2), 1–390.

Høydalsvik, F., C. Mauritzen, K. Orvik, J. LaCasce, C. Lee, and J. Gobat (2013). Transport estimates of the western branch of the norwegian atlantic current from glider surveys. *Deep Sea Research Part I: Oceanographic Research Papers 79*, 86–95.

Knudsen, M. (1905). *Contribution to the hydrography of the North Atlantic Ocean.* Reitzel.

Körtzinger, A., J. Schimanski, and U. Send (2005). High quality oxygen measurements from profiling floats: A promising new technique. *Journal of Atmospheric and Oceanic Technology 22*(3), 302–308.

Le Vine, D. M., S. Abraham, F. Wentz, and G. S. Lagerloef (2005). Impact of the sun on remote sensing of sea surface salinity from space. *1*.

Le Vine, D. M., G. S. Lagerloef, F. R. Colomb, S. H. Yueh, F. Pellerano, et al. (2007). Aquarius: An instrument to monitor sea surface salinity from space. *Geoscience and Remote Sensing, IEEE Transactions on 45*(7), 2040–2050.

Le Vine, D. M., G. S. Lagerloef, and S. E. Torrusio (2010). Aquarius and remote sensing of sea surface salinity from space. *Proceedings of the IEEE 98*(5), 688–703.

Le Vine, D. M., G. S. Lagerloef, S. Yueh, F. Pellerano, E. Dinnat, and F. Wentz (2006). Aquarius mission technical overview. In *Geoscience and Remote Sensing Symposium, 2006. IGARSS 2006. IEEE International Conference on*, pp. 1678–1680. IEEE.

Lellouche, J.-M., O. Le Galloudec, M. Drévillon, C. Régnier, E. Greiner, G. Garric, N. Ferry, C. Desportes, C.-E. Testut, C. Bricaud, et al. (2013). Evaluation of global monitoring and forecasting systems at mercator océan. *Ocean Science 9*(1), 57.

Madec, G. (2012). the nemo team. nemo ocean engine. *Note du Pôle de modélisation, Institut Pierre-Simon Laplace (IPSL), France* (27).

Majohr, J. and T. Buch (2006). Modelling, simulation and control of an autonomous surface marine vehicle for surveying applications measuring dolphin messin. *IEE Control Engineering Series 69*, 329.

Manley, J. E. (1997). Development of the autonomous surface craft âacesâ. In *OCEANS'97. MTS/IEEE Conference Proceedings*, Volume 2, pp. 827–832. IEEE.

Martin, M., A. Hines, and M. Bell (2007). Data assimilation in the foam operational short-range ocean forecasting system: a description of the scheme and its impact. *Quarterly Journal of the Royal Meteorological Society 133*(625), 981–996.

Martins, A., J. Almeida, A. Silva, and F. L. Pereira (2006). Vision-based autonomous

surface vehicle docking manoeuvre. In *MCMC2006 7th IFAC Conference on Manoeuvring and Control of Marine Craft, Lisbon*.

Mogensen, K., M. A. Balmaseda, and A. Weaver (2012). *The NEMOVAR ocean data assimilation system as implemented in the ECMWF ocean analysis for System 4*. European Centre for Medium-Range Weather Forecasts.

Mohn, H. (1878). The norwegian north atlantic expedition. *Nature 18*, 425.

O'Dea, E., A. Arnold, K. Edwards, R. Furner, P. Hyder, M. Martin, J. Siddorn, D. Storkey, J. While, J. Holt, et al. (2012). An operational ocean forecast system incorporating nemo and sst data assimilation for the tidally driven european north-west shelf. *Journal of Operational Oceanography 5*(1), 3–17.

Pascoal, A., P. Oliveira, C. Silvestre, L. Sebastião, M. Rufino, V. Barroso, J. Gomes, G. Ayela, P. Coince, M. Cardew, et al. (2000). Robotic ocean vehicles for marine science applications: the european asimov project. In *Oceans 2000 MTS/IEEE Conference and Exhibition*, Volume 1, pp. 409–415. IEEE.

Paskyaci, M. B. and I. Fer (2010). Ocean near-surface boundary layer: processes and turbulence measurements.

Peddie, D. (2011). The sailbuoy ocean vessel for metocean instrumentation. *ONT 17*(10), 30–31.

Perry, MJ, R. D. (2003). Observing the ocean with autonomous and lagrangian platforms and sensors (alps): The role of alps in sustained ocean observing systems. *Oceanography 16*(4), 31–36.

Pham, D. T., J. Verron, and M. C. Roubaud (1998). A singular evolutive extended kalman filter for data assimilation in oceanography. *Journal of Marine systems 16*(3), 323–340.

Sætre, R. (2007). *The Norwegian Costal Current - Oceanography and Climate*. Tapir Academic Press.

Sætre, R. (2012). Gullalderen i norsk havforskning. *Naturen 135*(3), 113–122.

Sætre, R. and R. Ljøen (1972). The norwegian coastal current.

Schmitt, R. W., R. Petitt, et al. (2006). A fast response, stable ctd for gliders and auvs. pp. 1–5.

Stark, J. D., C. J. Donlon, M. J. Martin, and M. E. McCulloch (2007). Ostia: An operational, high resolution, real time, global sea surface temperature analysis system. pp. 1–4.

Sundby, S. (2004). Går vi mot en ny istid?

Tengberg, A., J. Hovdenes, H. Andersson, O. Brocandel, R. Diaz, D. Hebert, T. Arneri-ch, C. Huber, A. Kortzinger, A. Khripounoff, et al. (2006). Evaluation of a lifetime-based optode to measure oxygen in aquatic systems. *Limnology and Oceanography methods (depuis 2003) 4*, 7–17.

Xu, T., J. Chudley, and R. Sutton (2006). Soft computing design of a multi-sensor data fusion system for an unmanned surface vehicle navigation. In *Proc. of 7th IFAC conference on manoeuvring and control of marine craft*.

Yueh, S. H. (2000). Estimates of faraday rotation with passive microwave polarimetry for microwave remote sensing of earth surfaces. *Geoscience and Remote Sensing, IEEE Transactions on 38*(5), 2434–2438.